Available online at www.sciencedirect.com
ScienceDirect
Coordination Chemistry Reviews 251 (2007) 401–428
COORDINATION CHEMISTRY REVIEWS
www.elsevier.com/locate/ccr

Review

The photophysics and photochemistry of cofacial free base and metallated bisporphyrins held together by covalent architectures

Pierre D. Harvey [a,*], Christine Stern [b], Claude P. Gros [b], Roger Guilard [b,*,1]

[a] *Département de Chimie, Université de Sherbrooke, Sherbrooke, J1K 2R1 Québec, Canada*
[b] *LIMSAG UMR 5633, Université de Bourgogne, 9 Avenue Alain Savary, BP 47870, 21078 Dijon Cedex, France*

Received 11 January 2006; accepted 15 June 2006
Available online 21 June 2006

Contents

Abstract

This review focuses on the photophysical properties of bisporphyrin systems held in a face-to-face configuration by covalent bonds via flexible or rigid spacers and metal–metal bonds. The cofacial arrangement induces intramolecular bismacrocycle interactions promoting basic photophysical events such as excitonic interactions and energy and electron transfers. These events are relevant to mimic light harvesting and reactor devices known for photosynthesis in plants, and can be monitored by luminescence and flash photolysis methods.

Keywords: Porphyrins; Fluorescence; Phosphorescence; Luminescence; Emission; Photophysics; Electron and energy transfer; Exciton

1. Introduction

It is well known that photosynthetic organisms convert solar energy into chemical energy with a very good efficiency. Since the discovery of the right structures of light-harvesting devices (LH1, LH2 and LH3) such as in the purple bacteria [1–7], many research groups have devoted efforts to mimic them (see for example Refs. [8–11]). The most common and versatile chromophore used in such studies is the porphyrin (Scheme 1).

This planar aromatic macrocycle is composed of four pyrrole residues held together by four *meso*-carbon atoms which can allow the metallation via four M–N coordination bonds onto the corresponding dianion and the functionalization at the *meso*- and β-positions. The LH1, LH2 and LH3 units exhibit wheel-shaped protein structures where side-by-side and almost cofacial arrangements (similar to J-aggregates or slipped dimers) of the chromophores (here chlorophyll) are observed. Investigations of the photophysical properties of dimers, trimers and larger oligomers held together by covalent and coordination bonds are numerous [8] and cover a whole series of various structures and arrangements going from assemblies to arrays. The key parameter of this geometry is the face-to-face configuration. This particular arrangement provides a unique way to place two chromophores at a given distance, inducing a through space energy

* Corresponding authors. Tel.: +1 819 821 7092; fax: +1 819 821 8017.
E-mail addresses: Pierre.Harvey@USherbrooke.ca (P.D. Harvey), Roger.Guilard@u-bourgogne.fr (R. Guilard).
[1] Tel.: +33 3 80 39 61 11; fax: +33 3 80 39 61 17.

0010-8545/$ – see front matter © 2006 Elsevier B.V. All rights reserved.
doi:10.1016/j.ccr.2006.06.009

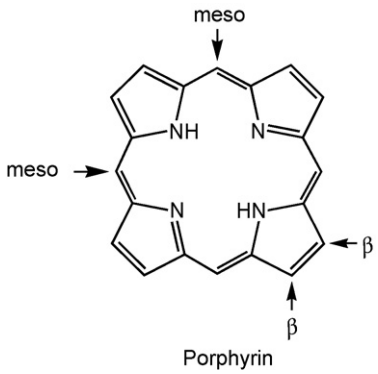

Scheme 1.

transfer as the shortest pathway for inter-macrocycle interactions and communications. We now wish to present an overview of the field, specifically devoted to the photophysical properties of cofacial systems.

2. Previous related reviews

There are several reviews (1999–today) [11–25], book chapters [8,26,27] and also a book [28] on the photophysics of free and metallated porphyrins, including electron (**et**) and energy transfers (**ET**), excitonic interactions, and photosensitization. During this recent period, most popular topics included polyporphyrin arrays (covalently bonded) [20,22,23,11] and assemblies built upon coordination linkages [12–19]. Other more general reviews have also appeared [21,25], and a more specific review on face-to-side dimers held together by a coordination bond was published in 2002 as well [24]. There is no review on covalently linked cofacial bisporphyrins so far. The reason probably lies in the very few examples reported, but many recent advances on the topic now justify an overview of these interesting bismacrocyclic systems. There are two categories of cofacial bisporphyrin molecules. First, the systems that are held together by flexible carbon chains, for which the photophysics were reported between 1985 and 1994, and secondly those using rigid spacers. The investigations of the photophysical properties of this "rigidly held bisporphyrins" series appeared more recently in the literature (a few papers in early 1990s, but many since 2001). The properties of these bisporphyrin macrocycles will be detailed. A review on the syntheses of these systems, more particularly focusing on improved routes for rigidly held bisporphyrins and related systems, was published in 2000 [28], and so no detail on the syntheses is presented in this review. This article also excludes bisporphyrin systems that are held together by M–X–M bridges (X = O and O_2, for instance) because any inter-macrocycle interactions are mediated by the coordination bridge, and also systems where the distance between the two macrocycles is more than 8–9 Å.

3. Review

3.1. Cofacial bisporphyrins held by flexible chains and "the early days"

The oldest report, excluding works on chlorophyll and bacteriochlorophyll, was published in 1977 by Chang [29], and concerns the bisporphyrins **1a**–**3a** (Scheme 2).

The complexation of these free bases **1a**–**3a** with Cu(II) provides **1b**–**3b** and the zero-field splitting constants were measured by EPR spectroscopy of the paramagnetic Cu(II) centers. The data indicate that these metals are interacting with each other. These constant values (0.0415, 0.0205 and 0.011 cm^{-1} for **1b**–**3b**, respectively) led to the evaluation of the M···M separations (4.2, 5.4 and 6.4 Å, respectively). The former value for **1b** corresponds to that estimated using a CPK model. The fluorescence quantum yield, Φ_F, for **1a**–**3a** are 0.007, 0.021 and 0.035, respectively, which are smaller than the standard monoporphyrin used, **4** ($\Phi_F = 0.094$) (Scheme 3) [29]. The decrease in Φ_F with the decrease in inter-macrocycle distance indicates self-quenching of the lowest energy excited state associated with intramolecular collisions and interactions. Evidence for excitons in **1a**–**3a** (2000–6000 cm^{-1}) based on the analysis of the Soret band was provided corroborating the presence of inter-porphyrin interactions.

Using the free base **1a**, the electron transfer dyad, **5**, and the corresponding model donor–donor dimer, **6**, were prepared (Scheme 4) [30].

The Mg-center is the electron donor and the free base is the acceptor. In these systems, attempts to measure the singlet excited state lifetime were made by flash photolysis. Because the charge separated species was formed well within the laser

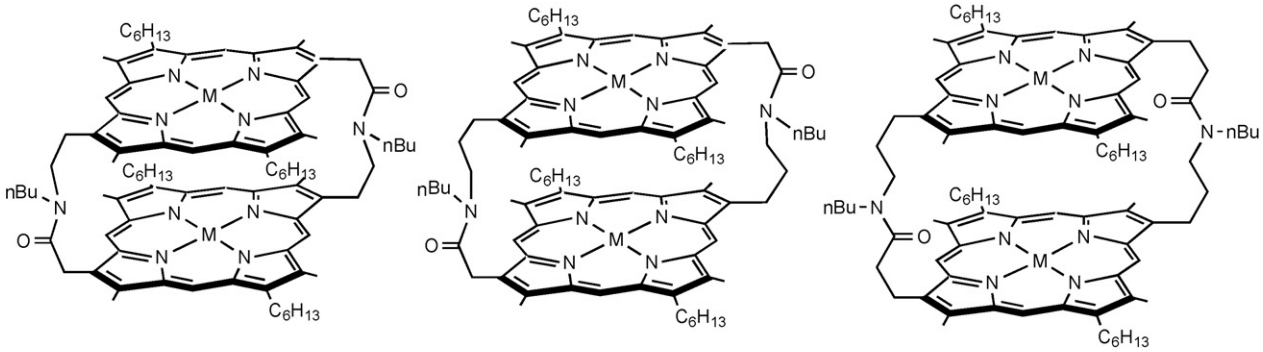

Scheme 2.

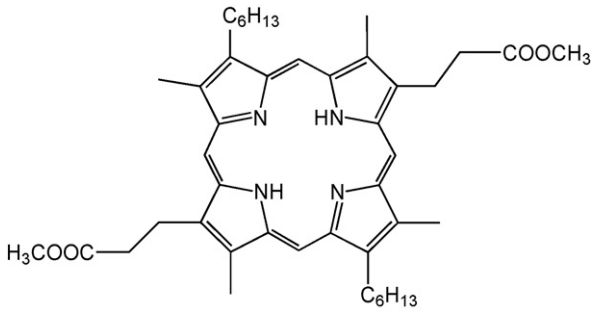

4

Scheme 3.

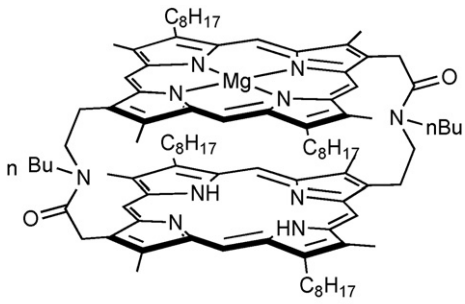

7

Scheme 5.

pulse (FWHM = 6 ps), the rate for this intramolecular **et** is higher than 10^{11} s^{-1}. The lifetime of the charge transfer (CT) is 620 ± 20 ps. Such a value is typical for efficient **et** in the singlet excited state [27]. These same research teams of Netzel et al. confirmed these excited state assignments by adding iodobenzene (heavy atom effect to populate the triplet state via an increase in intersystem crossing rate) and *p*-benzoquinone (as a competitive reaction test) to solutions containing the Mg/H_2 derivative **7** (Scheme 5) [31].

Dimer models **8** and **9** were also synthesized and characterized in order to investigate the cofacial trimer **10** (Scheme 6) [32]. The UV–vis spectrum of **10** in a toluene/pyridine (1:100) mixture and DMF consists approximately of a superposition of two Zn-containing porphyrins and a metal free porphyrin. The luminescence of **10** appears exclusively at 627 nm, a fluorescence attributed to the free base chromophore only. This result implies a rapid energy transfer from the Zn-containing chromophore to the free base acceptor.

Experiments were performed to demonstrate that the perturbation of the donor can be observed from the change in energy transfer rate and acceptor lifetime. Addition of Cl^- ions, as tetra-*n*-butyl ammonium salts in CH_2Cl_2/1% pyridine mixtures, was made. The Φ_F data for **10** are as follow: 0.046, 0.024, 0.014, and 0.018 for toluene/1% pyridine, CH_2Cl_2/1% pyridine/0.1 M TBAP (tetra-*n*-butyl ammonium perchlorate), CH_2Cl_2/1% pyridine/0.1 M TBAC (tetra-*n*-butyl ammonium chloride), and DMF, respectively. The τ_F data are 15.2, 12.5, 8.2, and 11.0 ns, respectively. Both series of data show that the fluorescence is quenched as the dielectric constant of the solvent increases, and that the fluorescence of **10** is mostly quenched by Cl^- ion-containing solutions. This observation implies that the quenching is due mainly to non-radiative depletion of the S_1 population of **10** rather than a large change in the radiative rate constant. Based on flash photolysis experiments, the triplet formation for **10** remains roughly constant.

In an attempt to model the efficient electron transfer and charge separation processes in photosynthesis, triad **11** as well as the model compounds **12** and **13** were prepared and investigated by means of fluorescence lifetimes (Scheme 7) [33]. One of the problems to be solved was the role of pair of chlorophylls, which are placed face-to-face in green plants and photosynthetic bacteria. In the charge separated state, the positive charge on the chlorophyll is believed to be delocalized over the pair of chlorophylls.

Triads **11**–**13** were synthesized and characterized such as the symmetrical dimer **13** which shows characteristic features of the special pair chlorophyll (P700; i.e. blue-shifting of the Soret band, red-shifting of the Q-bands, and lower redox potentials compared to monoporphyrin **14** (Scheme 8)). However, the interactions between the two macrocycles appear minimal [33] as the interchromophore distance is in the order of 5.4–6.4 Å [29]. The quinone acts as the electron acceptor in this triad model. No appreciable difference between 350 and 700 nm in the absorption spectra of **11**–**13** indicates that there is no interaction between the bisporphyrin fragment and the pendant group. Compound **11** exhibits in various solvents such as THF, dioxane,

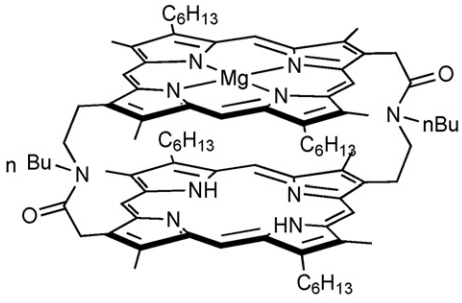

5

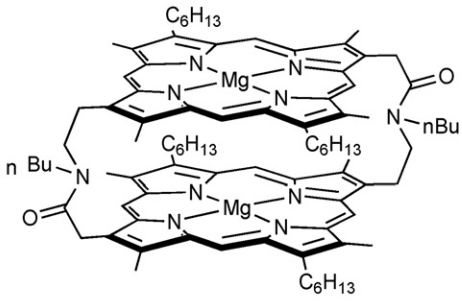

6

Scheme 4.

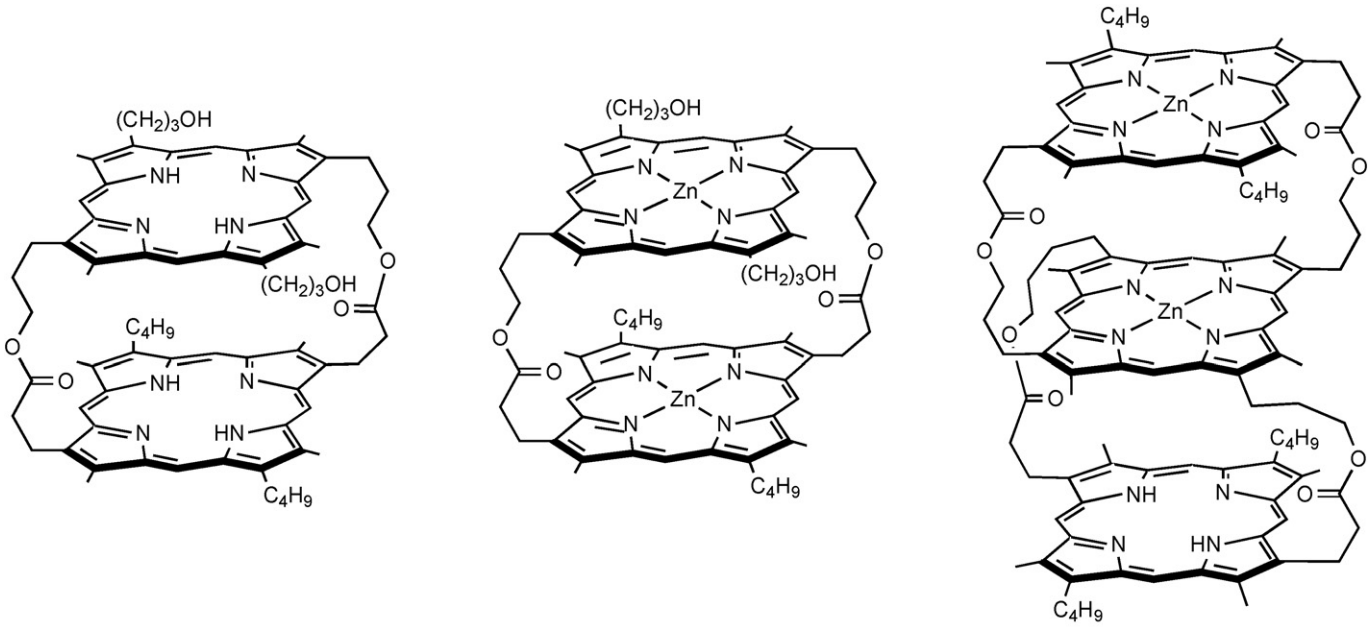

Scheme 6.

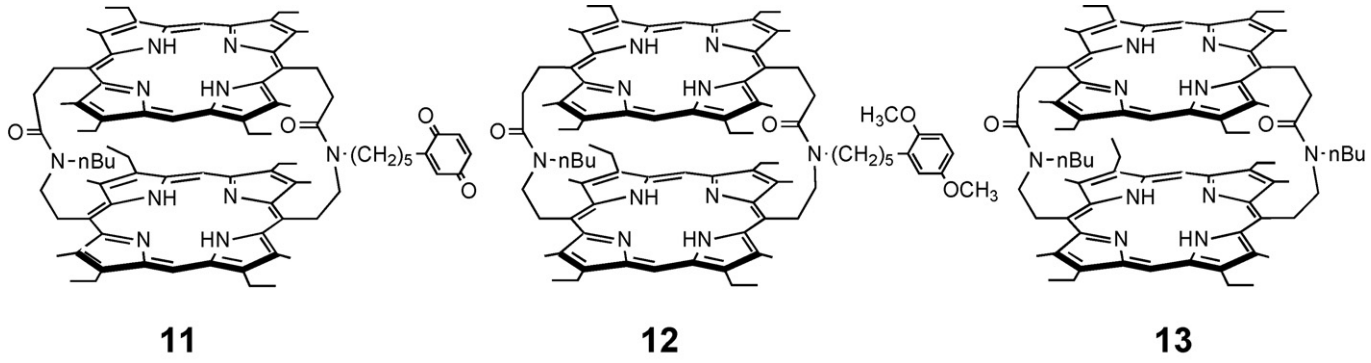

Scheme 7.

acetone, and benzene, a fluorescence intensity that is much less than that of **13**, suggesting the presence of an efficient photoinduced **et** from the bismacrocycle donor to the quinone. The latter bismacrocycle exhibits a τ_F of 10.1 ns in THF, while **11** exhibits a decay trace with three components (130 ps (100), 1.21 ns (10), 8.10 ns (8)), attributed to different conformers. The relative weights in parentheses seem to be affected, to some extent, by the nature of the solvent. For example, in benzene the data are 140 ps (100), 1.04 ns (22) and 6.76 ns (11), while in acetonitrile they are equal to 60 ps (100), 1.10 ns (30) and 5.12 ns (4).

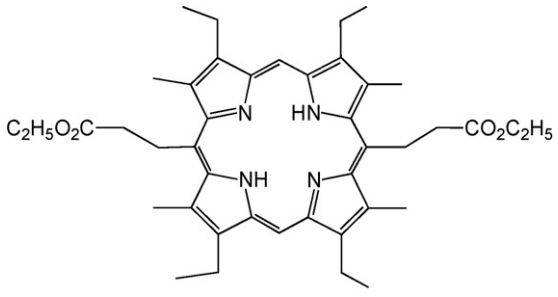

14

Scheme 8.

The problem of orientations and conformers was revisited by Sanders and co-workers 3 years later [34]. The face-to-face and side-by-side triads **16** and **17**, respectively, along with model **15** were investigated by means of ps transient absorption and emission experiments using the pyromellitimide as electron acceptor (Scheme 9). Both the excited singlet and charge separated states were established in **16** and **17** from ps transient absorption spectroscopy.

By setting a relative Φ_F of 1.0 for compound **15**, the Φ_F data for **16** and **17** are 0.005 and 0.24, respectively, indicating the importance of the relative orientation of the pair. The rate for the charge separation in **16** ($(1.1–3.6) \times 10^{11}\ s^{-1}$) is about 1000 times faster than that found for **17** ($(3.8–6.5) \times 10^{8}\ s^{-1}$). Energy

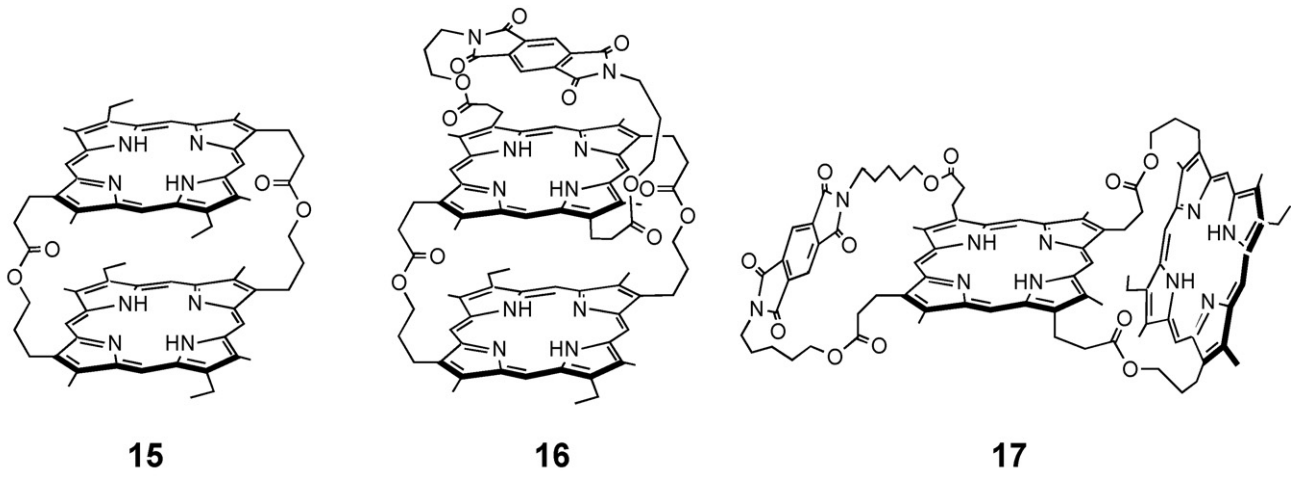

15 **16** **17**

Scheme 9.

transfer between the two porphyrin centers occurs. However, it is assumed to be fast in both cases. No evidence for multiple components in the decays and increases in charge separated intermediates were reported.

It is only in 1988 that it was recognized that the use of flexible spacers in bisporphyrins could lead to aggregates; stacking of the porphyrin rings being due to π–π interactions [35]. Compounds **18** and **19** exist as *meso* and racemic, and *syn* and *anti* isomers, respectively (Scheme 10).

Based on ^{1}H NMR, including NOE experiments and geometry computations, the structures for the cofacial dimers **18** (*meso* form) and **19** (*syn* form) were addressed (Scheme 11), and an offset was found (slipped dimers).

The broadening (about 57 nm wide), and blue- and red-shift of the Soret and Q-bands, respectively, relative to related monoporphyrins, confirm the presence of inter-macrocycle interactions, also called exciton coupling. The Φ_F data are 0.47 (λ_{em} = 626 nm), 0.54 (λ_{em} = 624 nm), 0.15 (λ_{em} = 586 nm), 0.20 (λ_{em} = 570 nm) for **18a**, **19a**, **18b** and **19b**, respectively. In a subsequent work, the disaggregation of **18b** and **19b** by basic ligands has a small electronic component, but is dominated by steric factors [36].

Dimers **20**–**22** are closely spaced quadruply bridged *meso*-substituted bisporphyrins (Scheme 12) [37]. Based upon computer modeling, notably on **20a** and **21a**, a face-to-face geometry with no offset is assigned. Some weak exciton coupling is noticed from the FWHM of the Soret band for **20a** and **22a** in $CHCl_3$ and DMSO. These values are about 19 nm while the *m*-(bromomethyl)tetraphenylporphyrin exhibits a FWHM value of 12 nm. The cavity is found to be too small to let a solvent molecule penetrate it.

Exciton couplings were also investigated for dimer **24** and trimer **25** (Scheme 13). The aim was to elucidate whether a pure exciton coupling effect or (and) a charge-transfer process could account for the change in photophysical properties in free base dimers and trimers with respect to the monoporphyrin **23** (Scheme 13) [38].

Indeed, the FWHM of the Soret band for **23**, **24** and **25** in DMSO for example, are 14.4, 21.8 and 27.0 nm, respectively. The Φ_F data are 0.13, 0.077 and 0.055, respectively, illustrating the correlation with the FWHM. However, the lifetimes, τ_F, only slightly decreases from **23** (11.6 ns in DMSO) to **24** to **25** (both 11.3 ns in DMSO). This result is consistent with the lower quantum yield of the triplet formation, Φ_T, for **24** and **25**

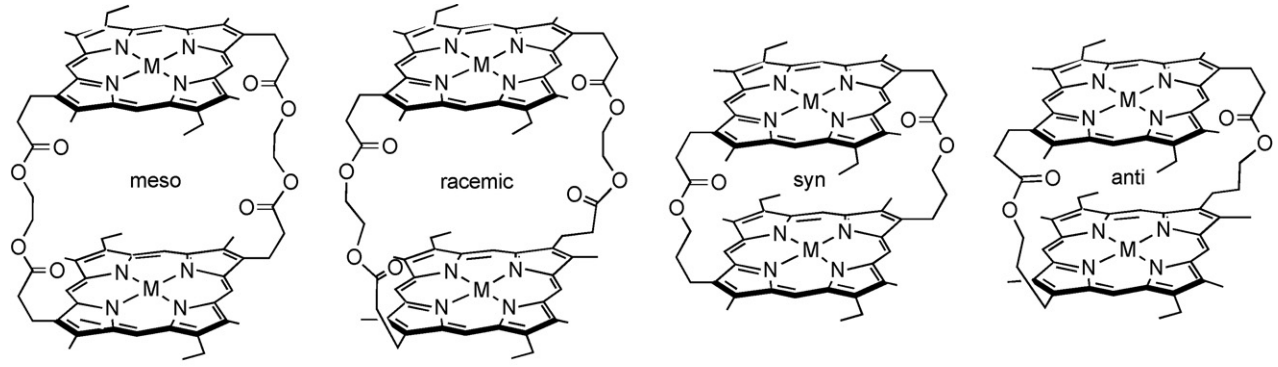

18a (M = H_2), **18b** (M = Zn) **19a** (M = H_2), **19b** (M = Zn)

Scheme 10.

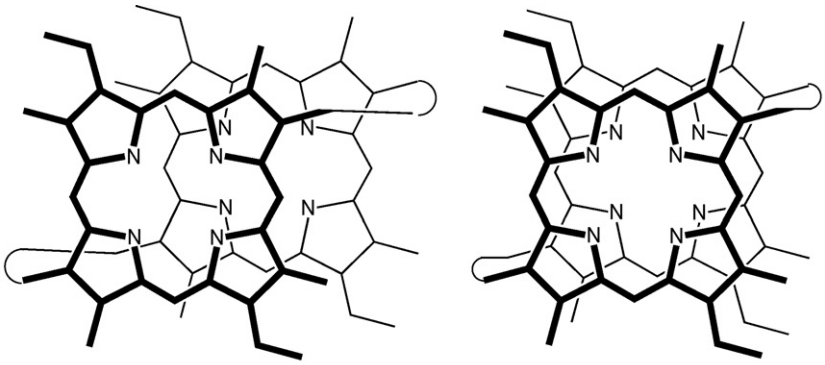

Scheme 11.

(both at 0.40 ± 0.05 in DMSO) with respect to **23** (0.85 ± 0.05 in DMSO).

The rate for photoinduced **et** (charge separation (CS) and charge recombination (CR)) in **7**, was investigated by means of ps transient absorption spectroscopy using different solvents [39]. The CS process is rapid ($k_{CS} > 2 \times 10^{11}\ s^{-1}$) for all cases, but k_{CR} is much slower (around $10^8\ s^{-1}$) and solvent-dependent. The slowness of CR, when compared to CS, was attributed to CR occurring in the inverted region of Marcus theory [31,40], but the rate constant for the CR does not correlate any common properties of the solvent such as the polarity. Instead, a nearly linear correlation between k_{CR} and $1/\tau_s$, where τ_s is the microscopic solvent relaxation time, is observed, even though k_{CR} ($10^8\ s^{-1}$) is much slower than the time scale for τ_s (10^{11} to $10^{12}\ s^{-1}$). This result is a predictable consequence of the reorganization energy when **et** and CR occur.

This dynamical solvent effect of the CR in the inverted region of Marcus theory was further investigated using dimers **7** (Scheme 5), **26**–**28** where chlorin residues were incorporated as electron acceptors in **26**–**28** (Scheme 14) [39,41]. The dimers exhibit different driving force for the CR ($\Delta G_{CR} = -1.9$ eV for **7** and **26**, and -1.6 eV for **27** and **28**). The rate constants, k_{CR}, are strongly solvent-dependent for all systems (**7**, $(0.6–4.0) \times 10^9\ s^{-1}$; **27**, $(1.6–8.3) \times 10^{10}\ s^{-1}$; **28**, $(1.0–4.6) \times 10^{10}\ s^{-1}$) and show a linear correlation with the solvent relaxation time (1.5×10^{10} to $1.6 \times 10^{12}\ s^{-1}$) for a same series of solvents. This solvent-dependence finds its origin in dynamic effects, with k_{CR} being governed by a diffusional activation barrier.

Sapphyrin is a macrocycle related to porphyrin, except it contains five pyrrole rings, and so, its absorption properties are expected to be different from its porphyrin congener. The pseudo dimer **29** exhibits a dyad structure where the donor, the porphyrin, and an acceptor, the sapphyrin, have a 0.19 eV energy difference between the S_1 excited states (Scheme 15) [42]. Excitation at 408 nm, where absorption of sapphyrin is minimal, gives rise to virtually no porphyrin fluorescence, but instead fluorescence from sapphyrin residue is observed. This photoprocess is attributed to an efficient S_1–S_1 **ET** from the porphyrin chromophore to the sapphyrin rings. Based on the observed intensity of the porphyrin donor and time-resolved fluorescence studies, the k_{ET} can only be estimated as $>2 \times 10^{10}\ s^{-1}$. The emission of the donor fluorescence was too weak to justify significant comments.

A recent original application is the host–guest properties of metallated bisporphyrin **30**, which exhibits a flexible ethane

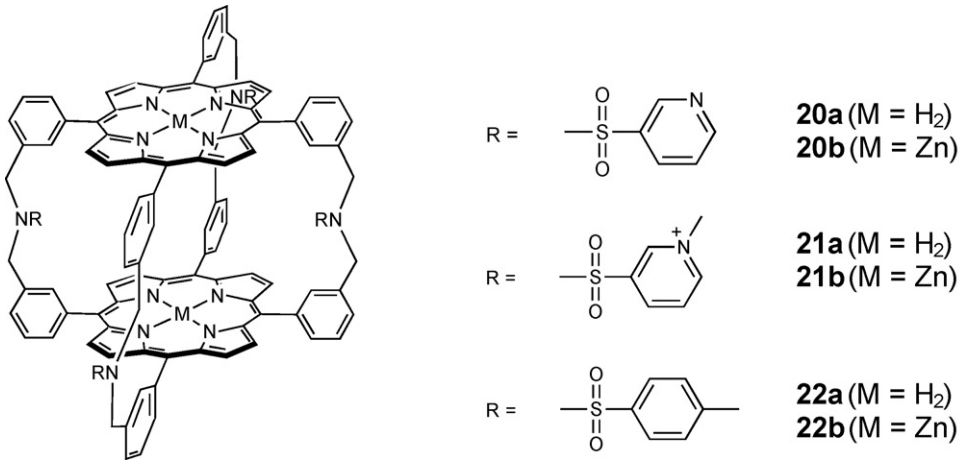

Scheme 12.

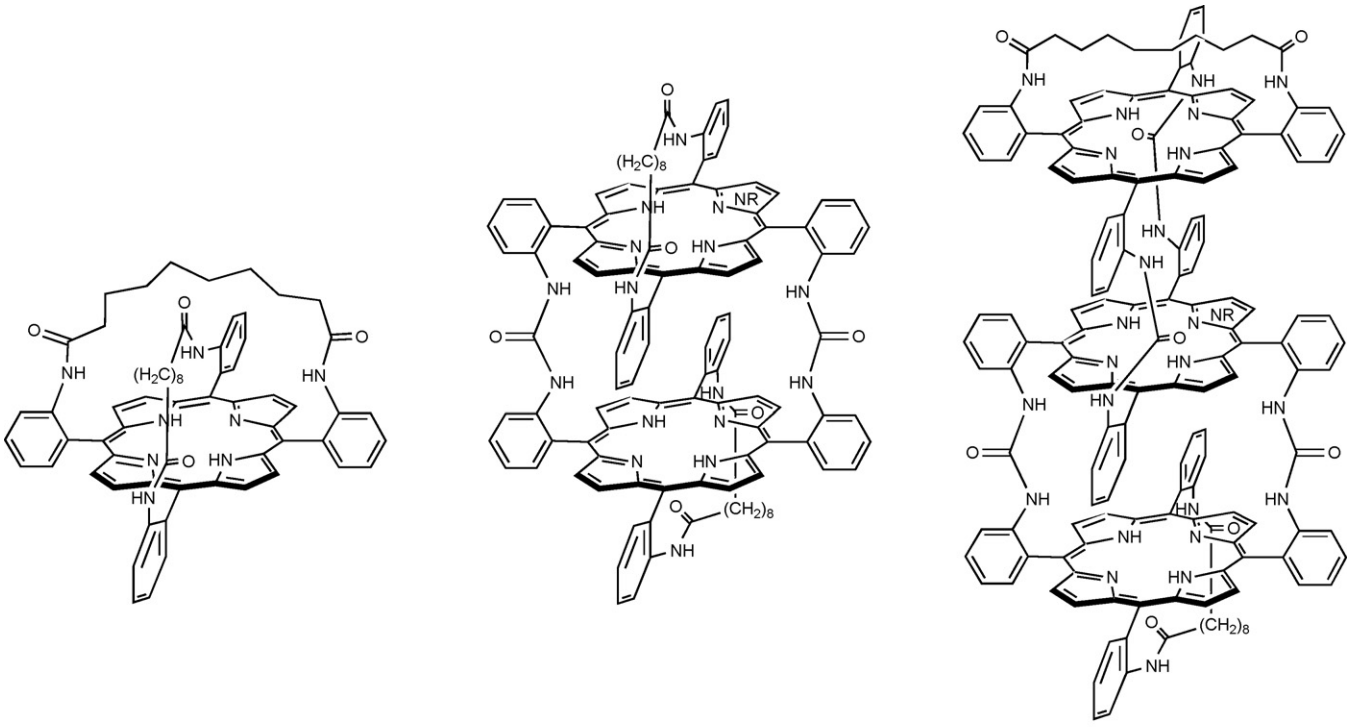

23 **24** **25**

Scheme 13.

spacer, towards chiral molecules [43]. Indeed, **30** is capable of binding a guest molecule, 1,2-diaminocyclohexane (both *R*,*R*- and *S*,*S*-isomers), as verified by circular dichroïsm (CD) and UV–vis spectroscopy (Scheme 16).

30·**Guest** was investigated by polarized fluorescence spectroscopy [43]. The induced chirality sign remains the same as that measured by CD spectroscopy in the region of the Q-band region. In addition, the fluorescence and absorption g factors are very similar, indicating the similarity of the host–guest structures of the ground and singlet excited states. Evidence for conformational stability is provided from the linearity of the mono-exponential fluorescence decay. A lifetime of 1.62 ns is measured, which is different from the non-coordinated monomer (1.79 ± 0.05 ns for OEP(Zn) in 2-MeTHF at 298 K [44]).

3.2. Cofacial bisporphyrins held by rigid spacers

The first photophysical study on rigidly held cofacial bis- and polyporphyrins appeared in 1991 [45,46]. Again, the investigation of the mechanism of the primary **et** processes in the photosynthetic materials and the role of the special pair (dimeric bacteriochlorophylls) was the purpose of these studies. The dyads and polyads **31a**–**33b** were prepared and investigated

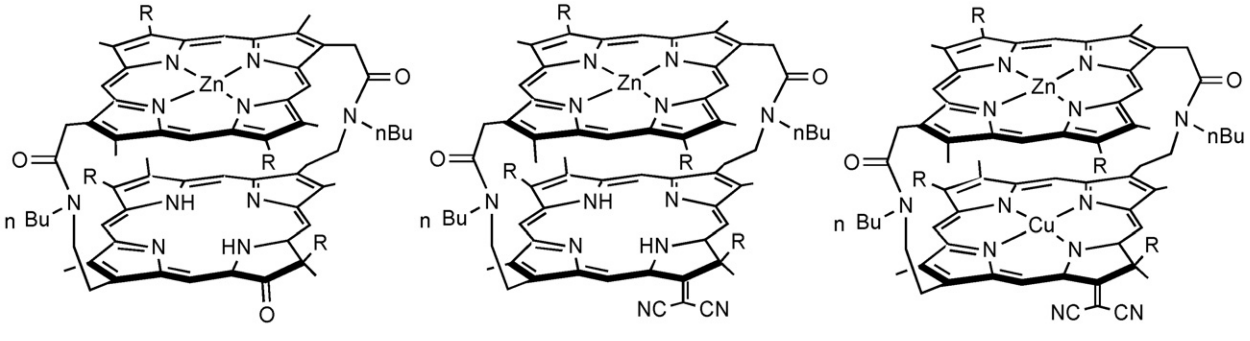

R = n-C_8H_{17} R = n-C_8H_{17} R = n-C_8H_{17}

26 **27** **28**

Scheme 14.

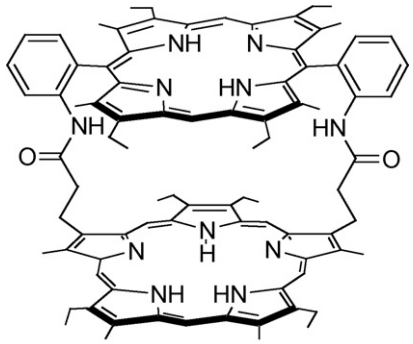

29

Scheme 15.

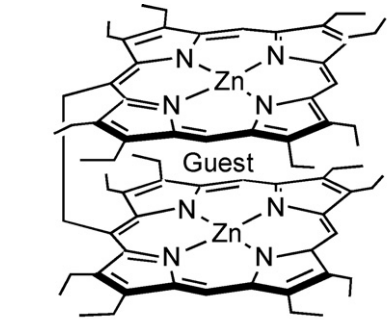

Guest = 1,2-diaminocyclohexane

30•Guest

Scheme 16.

(Scheme 17). The benzoquinone (bq) acts as the electron acceptor while the *p*-dimethoxyethylbenzene (hqe) acts as a redox inactive pendant group (the reduction potential is too high for this fragment to be involved). The effect of this pendant group is very similar to that of bq such that the quantitative impact of its presence on the photophysical parameters (loose bolt effect), beside **et**, is the same.

As preliminary results, the splitting of the Soret bands underscore strong and increasing exciton coupling going from **31a** to **32a** to **33a** indicates that this coupling is strongly related to the adjacent porphyrin unit more than the cofacial pair [45,46]. The Φ_F varies as <0.0005, 0.0019 and 0.0048, respectively. The fluorescence arising from the macrocycle adjacent to the quinone is significantly quenched [45]. This result corroborates the effect of the adjacent covalently bonded structure on the exciton coupling. In comparison with **32b** ($\Phi_F = 0.024$) and **33b** ($\Phi_F = 0.025$), the large decrease in Φ_F for **31a**–**33a** is clear evidence of quenching of all porphyrins (proximal and distal). This result means that **et** affects the whole molecule, including the cofacial pair and the adjacent chromophore to the quinone residue. The ps transient absorption study demonstrates the presence of rapid charge separation, CS (within the 24 ps duration of the YAG laser pulse), and rapid charge recombination, CR, for all cases in THF as the solvent (10^{11} s^{-1}). The presence of multi-components in the CR is attributed to competitive back **et** between the proximal and distal porphyrins. For example, the two components in the CR processes of **31a**, are 15 and 70 ps, respectively. For **33a**, the decay profile exhibits a 15- and a 500-ps component. The slower

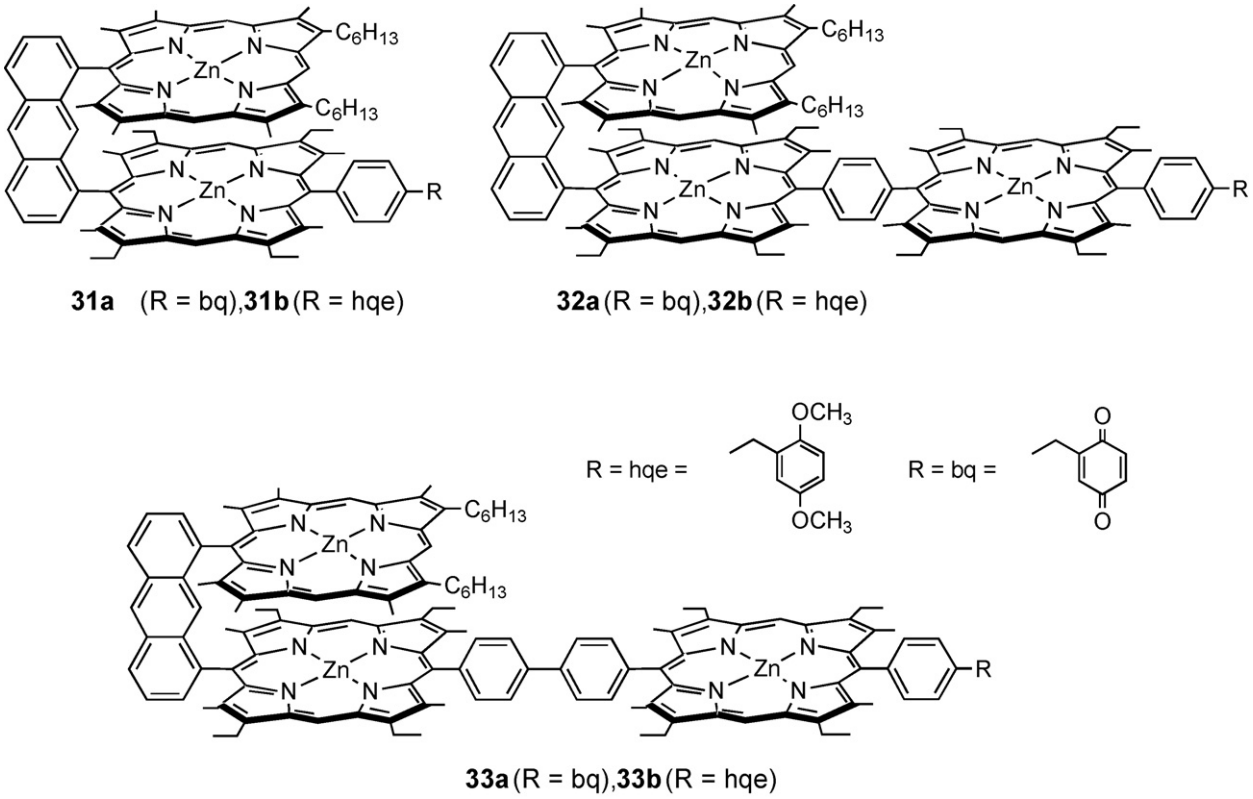

31a (R = bq), **31b** (R = hqe)

32a (R = bq), **32b** (R = hqe)

R = hqe =

R = bq =

33a (R = bq), **33b** (R = hqe)

Scheme 17.

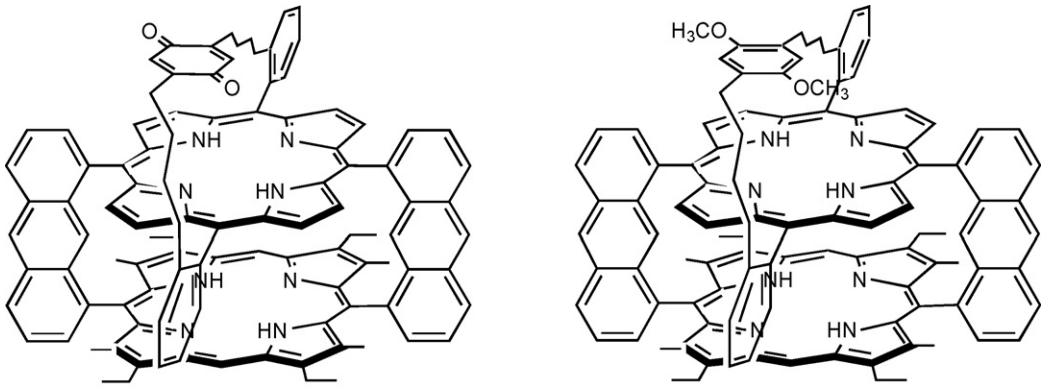

34 **35**

Scheme 18.

component is attributed to a CR process occurring between the quinone and the distal porphyrin.

In a related study, dimers **34** and **35** were synthesized in which the electron acceptor quinone was placed face-to-face with a rigidly held cofacial bisporphyrin dimer (Scheme 18) [47]. The particularity of these complexes is that the two porphyrin macrocycles are different, and so an **ET** process can occur in addition to **et** from two possible donors. Again, the absorption spectra of **34** and its model compound **35** are almost superimposable demonstrating the minimal electronic effect of the quinone on the chromophores. However, the spectra are not a simple superposition of spectra of the isolated porphyrins with the same substitution patterns. For example, the Soret bands of **34**–**35** for each chromophore are blue-shifted showing the inter-macrocycle electronic interactions between the two porphyrin units.

The relative Φ_F data (**34** versus **35**) which are 42% in *n*-hexane, 7% in toluene, and 2.5% in CH_2Cl_2, corroborate the change of τ_F in the same solvent. However, it was not possible to separate singlet–singlet inter bisporphyrin **ET** and bisporphyrin-quinone **et**. No subsequent report appeared since.

The first exhaustive photophysical study on cofacial bisporphyrins held by rigid spacers came only recently [48]. The series **36**–**42** (Scheme 19) in EtOH at 298 and 77 K exhibit π–π^* fluorescence arising from the free base and (GaOR)porphyrin moieties, while the (Co)porphyrin and (Ru(CO))porphyrin chromophores are not fluorescent. For example, **36** exhibits a vibrationally structured fluorescence band where the 0–0 band is located at 620 nm. τ_F and Φ_F are 14.2 ns and 0.020 at 298 K, and 24.0 ns and 0.044 at 77 K in ethanol; these parameters compare favourably to that of the unsubstituted monoporphyrin (15.3 ns and 0.054 in benzene at 298 K [49]).

Dyads **38** and **39** exhibit fluorescence arising from both the free base and the (GaOR)porphyrin macrocycles where the 0–0 peaks are depicted at ~620 and ~580 nm, respectively. This places the latter and former chromophores as singlet energy acceptor and donor, respectively. While the τ_F and Φ_F parameters remained about the same for the free base moiety in **38** and **39**, Φ_F of the (GaOR)porphyrin decreased with respect to that of **37** (by about an order of magnitude), suggesting the presence of singlet–singlet **ET**. At 298 K, no τ_F data could be reported for the (GaOR)porphyrin chromophore due to the limitation of the instrument (ns photon counting; FWHM = 3.0 ns), which only indicates that $\tau_F < 0.3$ ns (which is the limit of value obtained by this method after deconvolution). Dimer **37** exhibits τ_F in the order of several ns (see below). The comparison of τ_F of **37** with those of **38** and **39** indicates a decrease from ns time scale values to values < 0.3 ns. This decrease is also consistent with the decrease in Φ_F and supports the intramolecular singlet–singlet **ET** process hypothesis.

As stated, no fluorescence arising from the (Ru(CO))-porphyrin and (Co^{II})porphyrin fragments was detected in

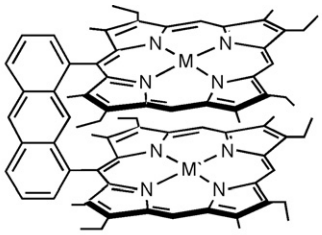

M	2H	Ga(OMe)	Ga(OMe)	Ga(OH)	Ga(OH)	Ga(OMe)	Ga(OH)
M'	2H	Ga(OMe)	2H	2H	Ru(CO)	Ru(CO)(MeOH)	Co^{II}
	36	**37**	**38**	**39**	**40**	**41**	**42**

Scheme 19.

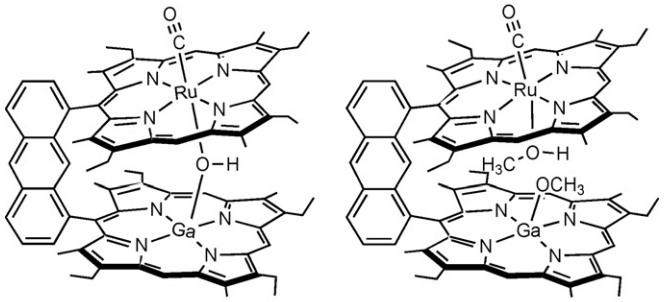

Scheme 20.

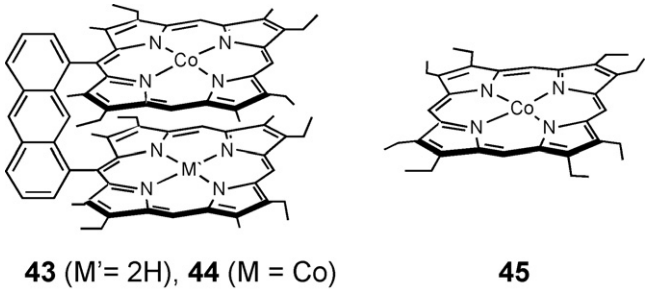

Scheme 21.

40–42 (Schemes 19 and 20). Instead, fluorescence from the (GaOR)porphyrin residue is observed at both 298 and 77 K where the 0–0 peak is observed at the typical position of 580 nm. **40** is phosphorescent at 77 K (λ_{max} = 709 nm; τ_P = 0.65 μs in 2-MeTHF), a phenomenon assigned to the (GaOH)porphyrin. The presence of phosphorescence in **40** may be due to spin–orbit coupling of the heavy Ru atom. For **42**, the presence of low-lying d–d states, from which molecules find ways to deactivate in a non-radiative way, is attributed to the lack (or large weakness) of phosphorescence and fluorescence.

Dimer **37** is particularly unusual since a double fluorescence is detected where the 0–0 peaks are located at 580 and 620 nm at 298 K in ethanol, corresponding to 0–0 bands in the absorption (572 and 600 nm). The ns time scale lifetimes (3.5 and 4.4 ns) observed for both signals confirm the fluorescence. No explanation was provided but the possibility of two isomers, depending on how the OR groups are placed outside–outside versus outside–inside, may be at the origin of this unusual behaviour. X-ray structures of **40** and **41** strongly support this hypothesis in which OH and OMe/L (L = MeOH), respectively, are found inside the cavity.

Subsequently, dyad **43**, dimer **44**, and monomer **45** were investigated with respect to O_2 binding and detection (Scheme 21) [50]. The unusual feature was found in **43** where, at 77 K in 2-MeTHF, very weak peaks at 552 and 590 nm were observed. The nature of these weak signals was quickly assigned by comparing them to spectra of **44** and **45**. These weak emissions (Φ_F = 0.00028 and 0.00027, respectively, for **44** and **45**) are due to (Co)porphyrin fluorescence, a photophysical property never observed before for such a chromophore. But in all cases, τ_F is very short (<0.3 ns).

However, upon oxidation by O_2 in the presence of imidazole as a coordinating ligand, complete quenching of the Co(porphyrin) fluorescence is observed. In this case, the O_2 binding is accompanied by an oxidation of Co^{II}(porphyrin) to Co^{III}(porphyrin). Again, the presence of low-lying d–d states may be responsible for the absence of luminescence.

A good O_2 sensor is found for dimer **46** (Scheme 22) [51]. Fluorescence was unambiguously detected for **46–48** for the first time for such a chromophore at both 298 and 77 K. Immediately located after the Q-bands, the vibrationally structured fluorescence exhibits a mirror image with the absorption where, at 77 K, the 0–0 peaks are found at ~445 nm (τ_F = 0.81 ns; $\Phi_F = 3.0 \times 10^{-4}$), ~555 nm ($\tau_F$ = 0.75 ns; $\Phi_F = 1.6 \times 10^{-4}$), and ~580 nm ($\tau_F$ = 0.47 ns; $\Phi_F = 0.9 \times 10^{-4}$) for **47**, **48** and **46**, respectively. At 298 K, the τ_F and Φ_F data are very similar to that at 77 K illustrating the presence of rigidity in these macrocycles. These Pd-containing species are also phosphorescent where the 0–0 peaks are depicted at ~655 nm (τ_P = 2.07 ms; Φ_P = 0.40), ~660 nm (τ_P = 1.69 ms; Φ_P = 0.14), and ~685 nm (τ_P = 2.09 ms; Φ_P = 0.013), for **47**, **48** and **46**, respectively (at 77 K for example), matching the weak singlet–triplet absorption bands are seen at 610, 590 and 622 nm (at 298 K), respectively.

Delayed fluorescence was detected for **47** and **48** at 298 K, but not for **46**, presumably because this signal is too weak. Both fluorescence and phosphorescence bands for **46** at 298 and 77 K are broader than for **47** and **48**, indicating the presence of intermacrocycle interactions in **46**. The presence of these interactions results also from the observation of the smaller Φ_F, Φ_P and τ_F in **46** with respect to **47** and **48**.

The sensitivity of **46–48** towards O_2 was examined for both fluorescence and phosphorescence under Ar, air, and O_2 atmospheres at 298 K [51]. The significant data are listed in Table 1. Two parameters are important in evaluating the sensing perfor-

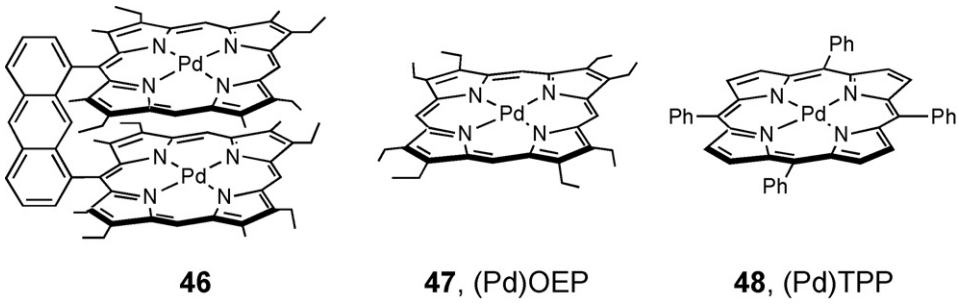

Scheme 22.

Table 1
Oxygen effect on the photophysical parameters [51]

	Φ_F (τ_F in ps)			Φ_P		
	Ar	Air	O_2	Ar	Air	O_2
46	3.35×10^{-4} (432)	1.15×10^{-4} (212)	0.44×10^{-4} (62)	0.0034	Not detected	Not detected
47	3.73×10^{-4} (685)	1.69×10^{-4} (554)	1.08×10^{-4} (477)	0.102	4.2×10^{-4}	5.5×10^{-6}
48	4.11×10^{-4} (665)	1.06×10^{-4} (479)	0.54×10^{-4} (330)	0.058	0.12×10^{-4}	Not detected

Table 2
Phosphorescence quenching data of **48**–**52** in 2-MeTHF at 298 K [52]

	k_Q ($\times 10^9$ M^{-1} s^{-1})	τ_P (μs)	K_{SV} ($\times 10^6$ M^{-1})	Lowest [O_2] detectable (ppm)
48	8.95	258	2.31	0.73
49	2.98	258	0.77	2.2
50	6.94	440	2.91	0.58
51	8.95	210	1.88	0.90
52	3.99	506	2.02	0.83

Table 3
Photophysical data for **48**, **52**–**55** in 2-MeTHF (fluo = fluorescence, phos = phosphorescence) [52]

	λ_{max} (nm)		Φ_{em}		τ_F (ns), τ_P (ms)	
	298 K	77 K	298 K	77 K	298 K	77 K
48 (phos)	696, 772	680, 755	0.020	0.17	258.7	1320
52 (phos)	699	688	0.0371	0.1551	506	1388
53 (fluo)	655, 719	615, 715	0.0686	0.1310	12.43	13.34
54 (fluo)	602, 654	611, 670	0.0284	0.0574	2.46	1.45
55 (phos)	–	729	–	<0.0001	–	45.5

mance of a luminescent molecule, Φ_e, and the variation of Φ_e and τ_e with [O_2]. Table 1 indicates that **47** and **48** are better sensors than **46** based on Φ_P.

A graph of Φ_e^0/Φ_e or τ_e^0/τ_e versus [O_2] (Stern–Volmer plots) gives a straight line where the slope (K_{SV}) relates the sensitivity of the emissive molecule towards O_2 [51]. By calculating the $\Phi_F(Ar)/\Phi_F(air)$, $\tau_F(Ar)/\tau_F(air)$, $\Phi_F(Ar)/\Phi_F(O_2)$, and $\tau_F(Ar)/\tau_F(O_2)$ ratios, one finds an equal or better sensitivity for **46** with respect to **47** and **48**. One concludes that the bimolecular quenching process could be more efficient if the trapping of O_2 inside the cavity is possible; this process must compete with all other unimolecular deactivation processes. This method of sensing O_2 is only applicable for fluorescence if adequate equipments are available. The use of the phosphorescence intensity is still the most convenient method to determine [O_2].

Further investigations on O_2 sensors included **48**–**52** demonstrating a collision-controlled phosphorescence quenching [52]. The bimolecular excited-state deactivation rate constants (k_Q) for quenching by O_2 and the Stern–Volmer constant (K_{SV}) for **48**–**52** are shown in Table 2. The very low value for **49** is easily explained by the mutual screening of the closely spaced macrocycles where there is no room for O_2 to penetrate inside the cavity and interact with the inner faces of the chromophores.

This relationship between k_Q and the surface area available for collision processes is also apparent for **51** and **52**. Fig. 1 shows the computed surface based on van der Waals radii for these two dimers where steric hindrance is clearly seen from the mesityl and tolyl groups, reducing the accessibility of the porphyrin chromophores to O_2.

For sensing purposes, K_{SV} (relative sensitivity with [O_2], $K_{SV} = \tau_P k_Q$) is larger for **48** and **50** than for **49**, **51** and **52**. The lowest [O_2] detectable with these sensors are 0.73, 2.2, 0.58, 0.90 and 0.83 ppm for **48**–**52**, respectively. While the best sensor is dimer **50**, the monomacrocycle **48** is still the most appealing option, considering the number of steps and chemical yields necessary to synthesize **50**.

Dimer **52** (Scheme 23), along with **53**–**55** (Scheme 24), were also prepared and characterized by emission spectroscopy and photophysical methods [52]. Their photophysical properties are presented in Table 3.

No evidence for Cu^{II}–Cu^{II} interactions was observed by EPR spectroscopy when analyzing the signal at half-field transition of **55**, suggesting that the Cu···Cu distance is greater than 6–7 Å [53]. This observation is consistent with the C_{meso}–C_{meso} distance observed for the dibenzothiophene spacer [52], and the

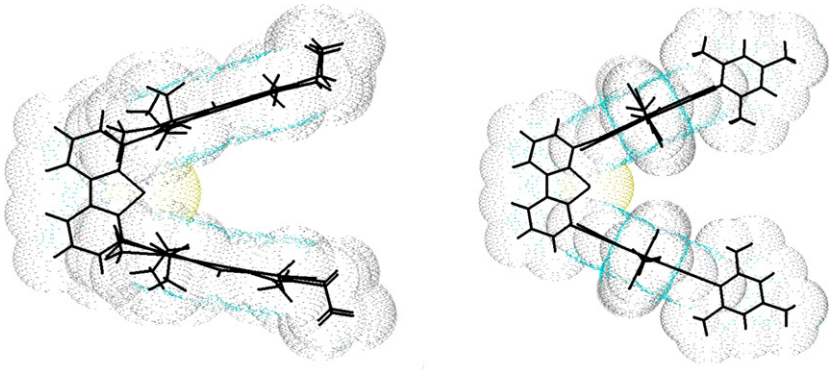

Fig. 1. Computed surfaces for **51** (left) and **52** (right) (PC-Model).

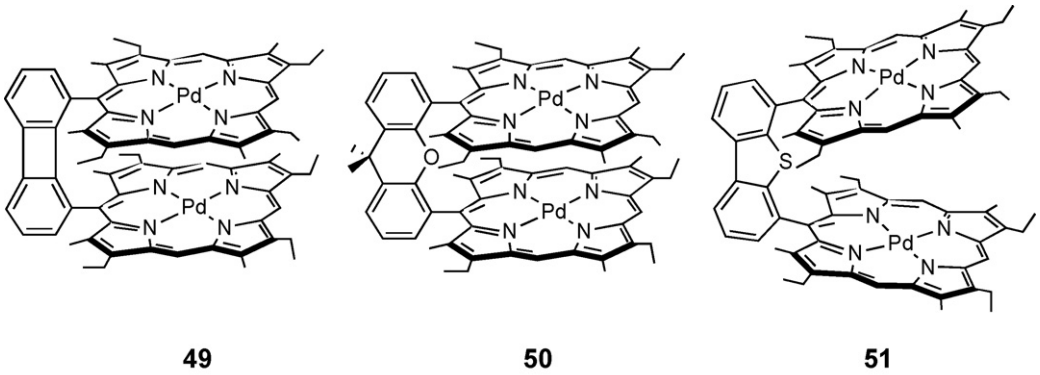

49 **50** **51**

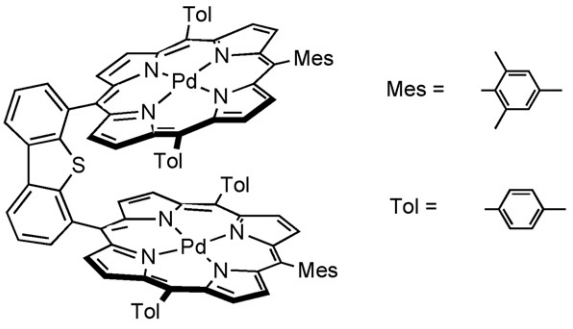

52

Scheme 23.

steric interactions between the *meso*-groups preventing macrocycle close contacts.

A study of the effect of the rigid spacer on the photophysical properties of the free base bisporphyrins **36**, **56**–**59** has been recently described (Scheme 25) [54]. A clear variation of τ_F and Φ_F is observed in Table 4. The trend is that both τ_F and Φ_F decrease as the distances between the two porphyrin centers (C_{meso}–C_{meso} (c–d) and CC_{meso}–CC_{meso} (a–b) distances) decrease. These parameters are obtained from averages obtained by X-ray structures for free base and metallated bisporphyrins. So the radiative (k_F) and non-radiative (k_{nr}) rate constants are directly related to the structural parameters. As the rings get closer to each other, they interact more strongly, and so deactivate one another more. The presence of inter-macrocycle interactions is evident from the comparison of the absorption and fluorescence bands. Indeed, the bands get broader as one goes from **59** to **58** to **36** to **57** to **56**.

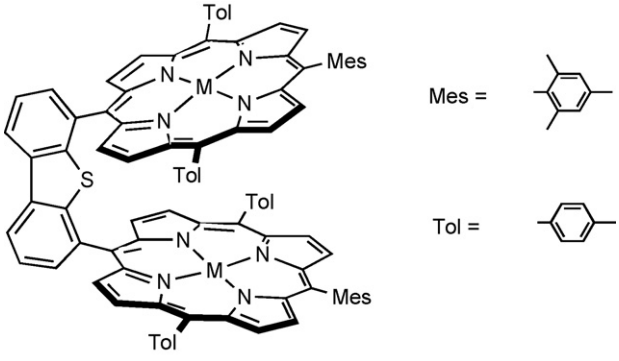

53 (M = 2H), **54** (M = Zn), **55** (M = Cu)

Scheme 24.

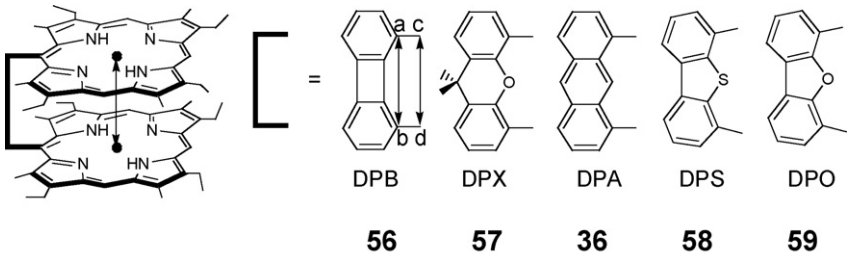

56 **57** **36** **58** **59**

Scheme 25.

Table 4
Photophysical parameters and bimolecular O_2 quenching data of **36**, **56–59** in 2-MeTHF at 298 K [54]

	τ_F (ns)	Φ_F	k_F ($\times 10^6$ s^{-1})	k_{nr} ($\times 10^7$ s^{-1})	k_Q ($\times 10^{10}$ s^{-1} M^{-1})
56	10.0	0.0040	0.40	10.0	0.9
57	12.4	0.011	0.80	8.0	1.4
36	14.1	0.020	1.4	6.9	1.7
58	16.9	0.035	2.2	5.7	1.6
59	17.7	0.045	2.5	5.4	1.4

The rates for bimolecular fluorescence quenching (k_Q) by O_2 can be divided into two families, **56** and **36**, **57–59**, respectively. The lower k_Q value observed for **56** suggests that the cavity is not accessible to O_2. This observation corroborates the data discussed above for the phosphorescence quenching of **49–51** (i.e. k_Q follows **49 < 50 < 51** (Table 2) as well as **56 < 57 < 58** (Table 4)).

Although the photophysics of the related series of cofacial dimers **60–66** was not reported in the article on optical properties and electronic structures described by Fletcher and Therien [55] (Scheme 26), their relevance to this review is obvious. These bis-macrocycles were cleverly prepared from the [2 + 2 + 2] cycloaddition of the corresponding ethynyl-bridged (zinc)bisporphyrins with 1,6-heptadiene in the presence of $Co_2(CO)_8$. The β–β isomers may exists as two atropisomers (*E* and *Z*) and the *meso*–β one can exist as two enantiomers.

It is interesting to note that previous to this work, X-ray structures of related 1,2-phenylene-bridged porphyrin macrocycles (such as **67**, for example [55–59]) indicate the presence of largely cofacial conformations when non-coordinating solvents are used to obtain crystals suitable for X-ray analysis [55–59]. Computer modeling and X-ray structures indicate sub-van der Waals contacts with distances of less than 3 Å [55]. Shifts in the 1-electron oxidation and reduction waves in the cyclic voltamograms between the dimers (**60–66**) and the corresponding monoporphyrins, are observed [55]. The three series of isomers (*meso–meso*, *meso*–β and β–β) exhibit perturbations of the properties when comparing monomers with dimers. For

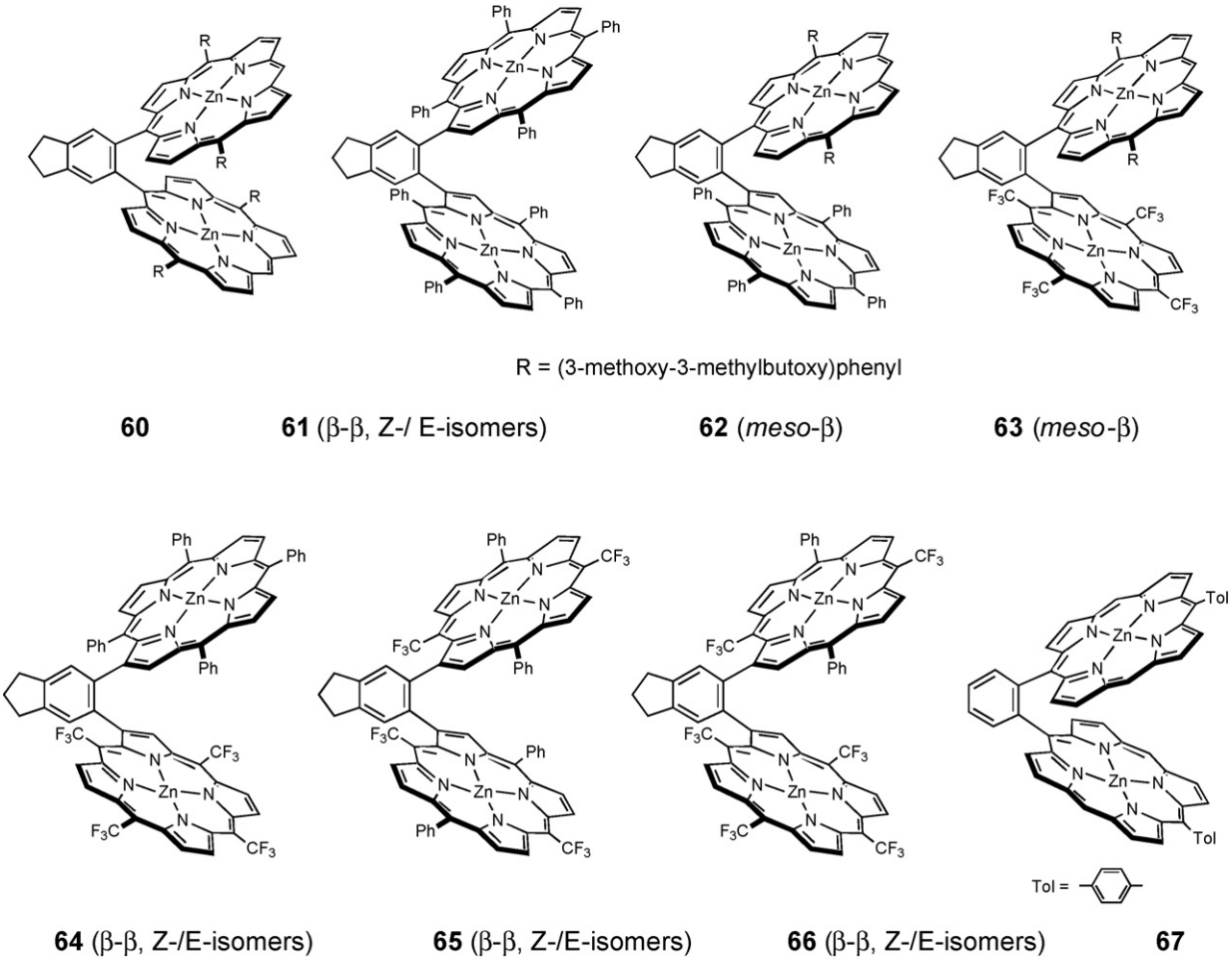

60 **61** (β-β, Z-/ E-isomers) **62** (*meso*-β) **63** (*meso*-β)

64 (β-β, Z-/E-isomers) **65** (β-β, Z-/E-isomers) **66** (β-β, Z-/E-isomers) **67**

Scheme 26.

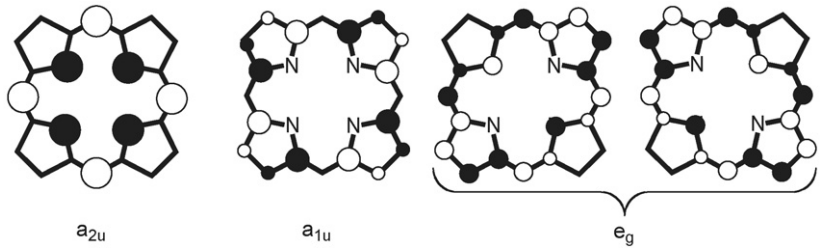

Fig. 2. Qualitative frontier MO descriptions based on Gouterman models [60].

Table 5
Fluorescence data for **57**, **59**, **68–71** in CH_2Cl_2 at 298 K [61]

	λ_{em} (nm)	Φ_F	τ_F (ns)
57	637, 671, 703	0.0298 ± 0.0090	10.55 ± 0.01
59	628, 658, 694	0.087 ± 0.010	10.70 ± 0.10
68	591, 640	0.0084 ± 0.0010	1.35 ± 0.01
69	578, 631	0.0541 ± 0.0010	1.50 ± 0.02
70	623, 649, 674, 689	0.1200 ± 0.0080	11.50 ± 0.10
71	572, 625	0.0298 ± 0.0090	1.45 ± 0.01

Table 6
Quantum yields for Scheme 28 for four phosphites in benzene at 298 K [61]

Phosphite	Cone angle (°) [61]	Quantum yield	
		(Fe_2O)DPX **72**	(Fe_2O)DPO **73**
$P(OMe)_3$	107	$9.0(1) \times 10^{-8}$	$7.4(7) \times 10^{-4}$
$P(OEt)_3$	109	$5.0(1) \times 10^{-8}$	$3.2(4) \times 10^{-4}$
$P(O^iPr)_3$	130	No reaction	$2.2(2) \times 10^{-5}$
$P(OSiMe_3)_3$	>172	No reaction	$2.2(3) \times 10^{-6}$

example, the degree of stabilization due to porphyrin–porphyrin interactions for the second steps of the first oxidative process is 130, 95, and 70 mV for **60–62**, respectively. The data were qualitatively interpreted with the description of the macrocycle-localized four Gouterman orbitals (Fig. 2) [60]. The a_{2u} and a_{1u} are the HOMO and HOMO-1. The a_{2u} orbital is the HOMO and a_{1u} the HOMO-1 when the *meso*-position is substituted by an aryl group. For H or an alkyl group in *meso*-position, the order is reversed. The LUMO is the e_u orbital in both cases. Close contacts clearly favour HOMO–HOMO and LUMO–LUMO interactions.

Nocera and collaborators reported the spectroscopic and photophysical data for the homo-dimers **57**, **59**, **68–71** in CH_2Cl_2 at 298 K as listed in Table 5 (Scheme 27) [61]. The comparison of the absorption and fluorescence spectra of **71** versus **69** versus **68** shows an increase in bandwidth, particularly for **68**, consistent with two strongly interacting porphyrins (exciton coupling). The photophysical data of Table 5 also show a decrease in τ_F and Φ_F for the DPX series (**57** and **68**) relative to the DPO and monoporphyrin congeners.

The μ-oxo dimers **72** and **73** were also prepared and investigated for their photoinduced oxidation reaction of phosphites (Scheme 28) [61]. Both dimers are thermally inert towards the phosphites, but upon irradiation an atom transfer reaction occurs. The presence of the phosphine oxide is demonstrated by ^{31}P NMR. The quantum yields of photoreaction are presented in Table 6. First of all, dimer **72** is much less reactive than **73**, indicating that the smaller cavity slows down the reaction by steric hindrance. The quantum yield is also dependent of the phosphite cone angle [61]; the reaction is slower as the cone angle increases, which is consistent with the steric hindrance model.

This steric hindrance hypothesis was supplemented by a contribution coming from a spring mechanism created by the spacer-(iron)porphyrin-oxo-(iron)porphyrin ring stress [62]. By examining the UV–vis spectra of (Fe_2O)DPX **72** and (Fe_2O)DPO **73**, for instance, a broad absorption appears at 360 nm which is due to a LMCT arising from a charge transfer

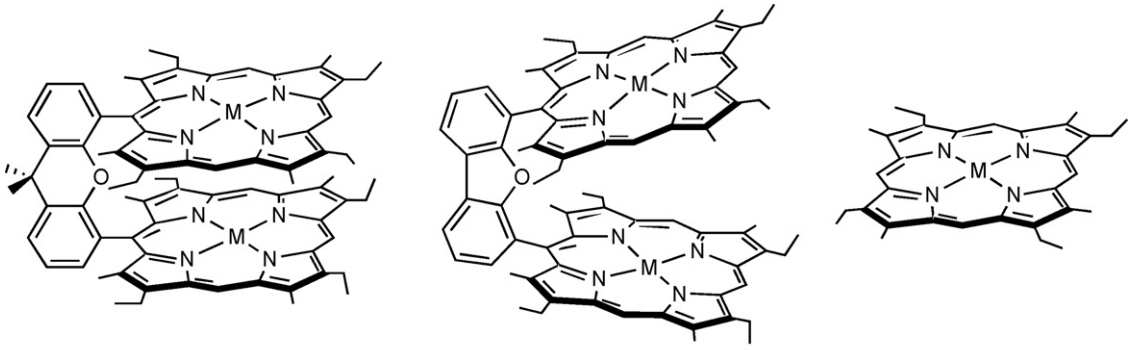

Scheme 27.

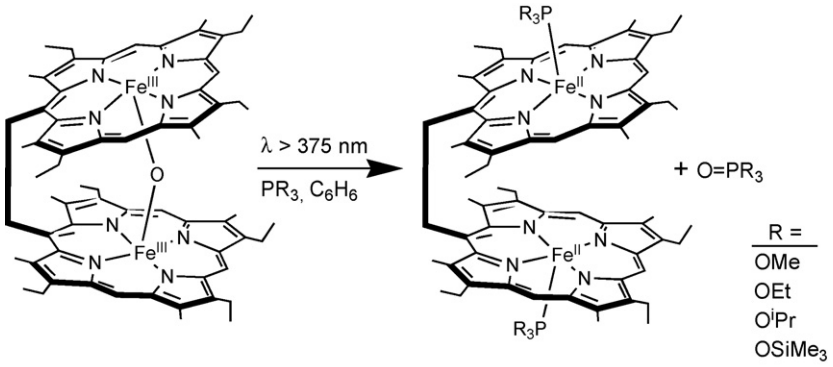

72 (spacer = xanthene, (Fe_2O)DPX)
73 (spacer = dibenzofuran, (Fe_2O)DPO)

Scheme 28.

going from the oxo-bridge to one of the iron(III) centers. In doing so, an Fe(II)/Fe(III) intermediate is generated in which the •O–Fe(II) bond is weaker compared to •O–Fe(III). This intermediate evolves through a second **et** from the Fe(III) center to the •O atom forming a ferryl/ferrous, O=Fe(IV)/Fe(II), intermediate. This assignment is based on an examination of the ps transient absorption spectra in the 20 ps to several ns range (the time duration of the laser pulse is 100 fs at 405 nm), and transient Raman studies where a $\nu(Fe^{IV}{=}O)$ band is observed at 852 cm^{-1}. This intermediate is formed within 20 ps, a fast rate consistent with the spring effect. This time frame is called τ_{spring}. In addition to **72** and **73**, dimers **74** and **75** were examined in order to verify the spring effect in the presence of bulky substituents at the *meso*-positions (in **74**) and the absence of ring stress (in **75**) (Scheme 29).

In all cases, no photoinduced decomposition is observed upon prolonged exposure to laser irradiation. The time of recovery of the bleached Soret band, which represents the time necessary to regenerate the starting material ($\tau_{reclamp}$), is 1.26(5), 1.36(3), 1.27(9) and 0.97(3) ns for **72**–**75**, respectively. This corresponds to rates of reclamping ($k_{reclamp} = 1/\tau_{reclamp}$) of $7.9(3) \times 10^8\ s^{-1}$, $7.4(2) \times 10^8\ s^{-1}$, $7.9(6) \times 10^8\ s^{-1}$, $10.3(4) \times 10^8\ s^{-1}$, respectively. This is a surprise since these values are essentially identical. No explanation is available yet. The overall photophysical process is shown in Scheme 30.

In the presence of a substrate, such as $P(OPh)_3$, the rate for photoinduced oxygen atom transfer reactivity (k_{OAT}; Scheme 28) was measured for dimers **74** and **75** and was compared to **72** and **73**. These are respectively, $9(1) \times 10^4\ s^{-1}$, $1.3(1) \times 10^7\ s^{-1}$, $1.4(1) \times 10^3\ s^{-1}$ and $1.1(1) \times 10^7\ s^{-1}$, which allows to place k_{OAT} in an increasing order according to **72** > **74** > **73** > **75**. This trend exactly follows the size of the cavity in the non-coordinated systems (extracted from X-ray data of other metallated bismacrocycles; see Ref. [62]). For the unbridged species **75**, the photo-cleaved fragments are unable to escape the solvent cage and retain the face-to-face geometry. In that respect, a Pacman-like pocket is retained even when the two porphyrins are not covalently attached. The vertical span of the pocket formed by the two monoporphyrins probably resembles that of the solvent cage in the DPO system (**73**), and is responsible for the lack of decomposition. It is also interesting to note the 10,000-fold increase in k_{OAT} from **72** to **73**; i.e. DPX to DPO-systems illustrating steric hindrance and spring effects on the reactivity of these cofacial bisporphyrin scaffolds.

The photoinduced oxidation of sulfides at 298 K can also be performed [63]. Indeed, **72**, **73** and **75** can be used to catalytically convert dimethyl sulfide (DMS) into dimethyl sulfoxide (DMSO) in the presence of air in the same manner as presented in Scheme 28 (except PR_3 is SMe_2 and $O{=}PR_3$ is $O{=}SMe_2$; see Scheme 30). The identity of the final bisporphyrin photoproduct is confirmed by the comparison of the resulting UV–vis spectrum after complete photochemical reaction with the spectrum of the independently prepared $(Fe_2)DPO{\cdot}(DMS)_2$. The presence

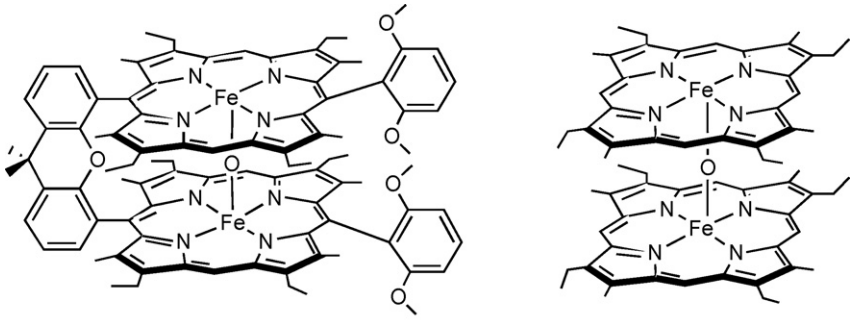

74 **75**

Scheme 29.

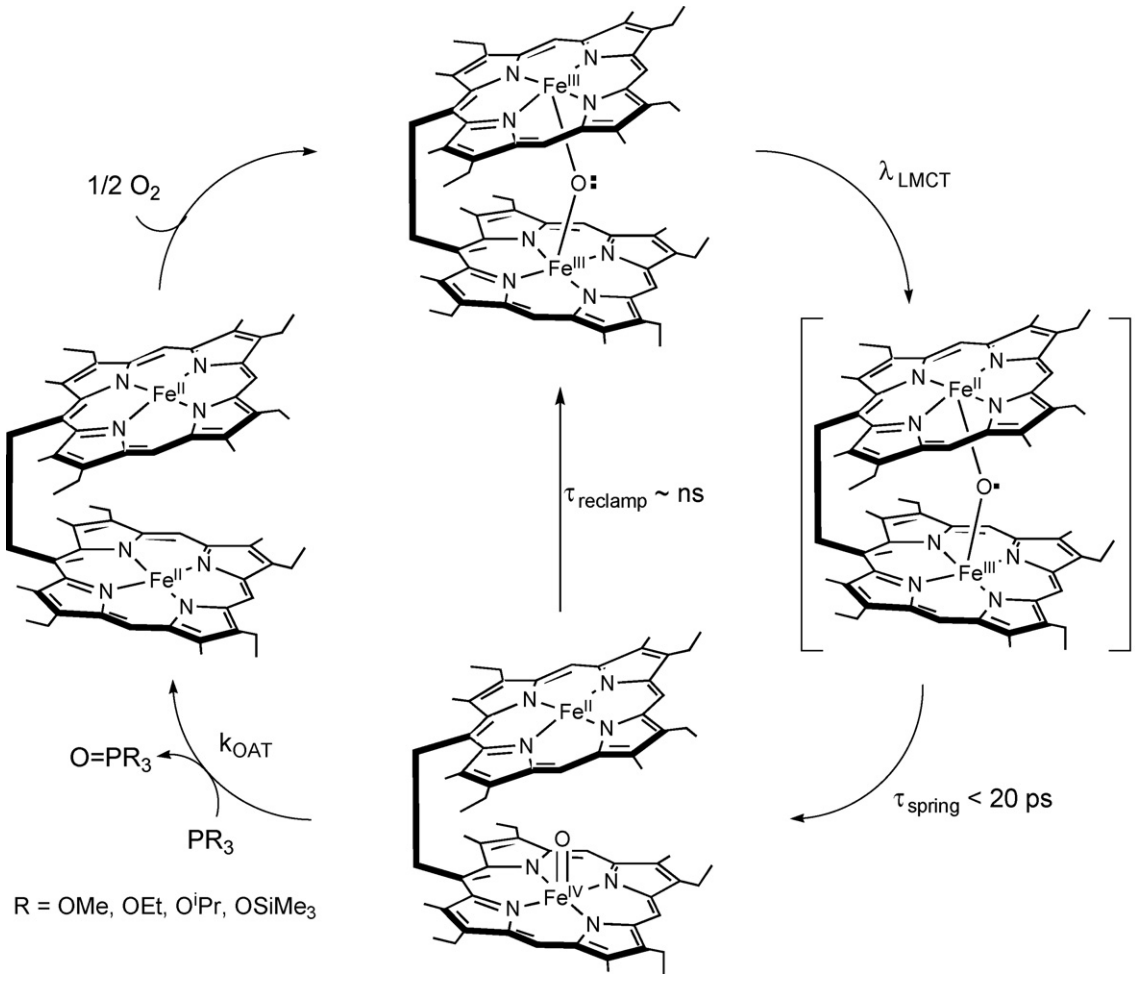

Scheme 30.

of DMSO is demonstrated by ^{1}H NMR and GC–MS. The quantum yield for the appearance of the photoproducts is 1×10^{-8}, 2×10^{-5} and 1×10^{-4} for **72**, **73** and **75**, respectively; a range that spans over three orders of magnitude. The turnover number (TON) follows this same trend (280 ± 14, 610 ± 31 and 350 ± 18, respectively). This comparison illustrates the spring effect in these cofacial bismacrocycles. The resemblance in quantum yields and TON between **72** and **75** is also consistent with the data described above for the Me_3P and the solvent cage effect. A small amount of dimethyl sulfone (Me_2SO_2, 5–12%) is also detected (1 atm of O_2).

The cofacial μ-oxo bisporphyrin dimer, **76**, also exhibits a catalytic photoinduced atom transfer reactivity, useful to oxidize olefins in epoxy molecules (Scheme 31) under mild conditions

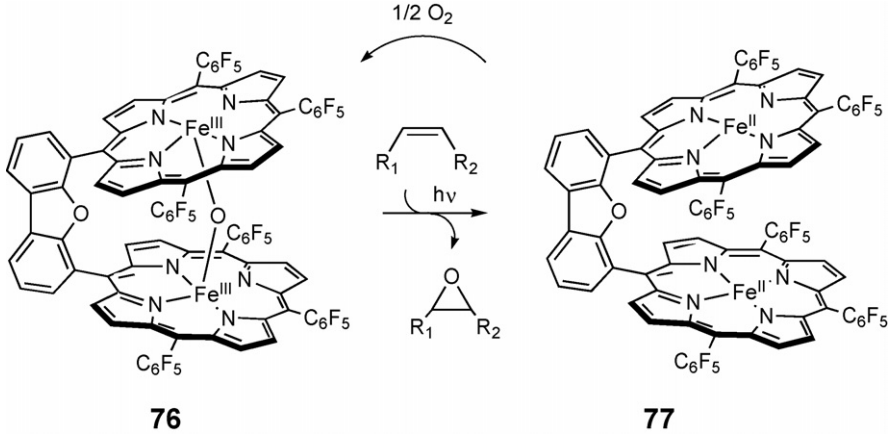

Scheme 31.

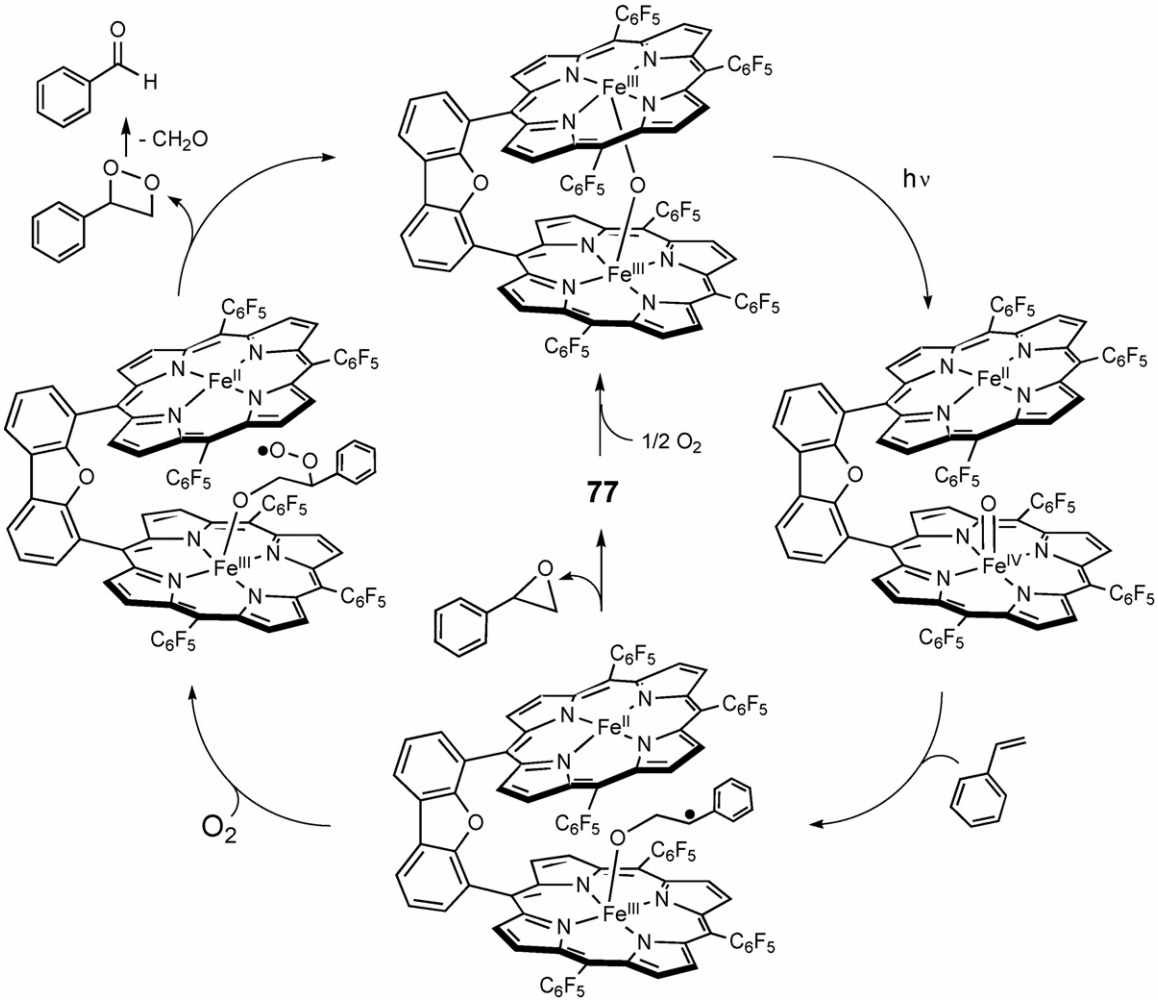

Scheme 32.

and visible light irradiation ($\lambda_{exc} > 425$ nm) [64]. The use of β- or *meso*-perfluorophenyl groups enhances the oxidizing properties of the metalloporphyrins and the possible oxidative damage to the porphyrin ring. For comparison purposes, **76** is also capable of catalyzing the oxidation of Me_2S into $Me_2S{=}O$, with an unprecedented TON (9635 ± 165 (~100% conversion)). No Me_2SO_2 is detected in this case.

In the case of olefin substrates, Scheme 31 does not proceed cleanly, but secondary products are observed after 4 h of photolysis at $\lambda_{exc} > 425$ nm [64]. For cyclohexene, the photoproducts are cyclohexene oxide (15%, TON = 89 ± 17), 2-cyclohexen-1-ol (12%, TON = 69 ± 12), and 2-cyclohexen-1-one (73%, TON = 437 ± 74). For styrene, these are styrene oxide (2%, TON = 37 ± 6), benzaldehyde (87%, TON = 1609 ± 340), acetophenone (8%, TON = 150 ± 27) and phenylacetaldehyde (3%, TON = 54 ± 11). The product distribution is consistent with radical type reactivity for organics. Scheme 32 presents the "proposed" photoinduced catalytic cycle that accounts for the presence of the epoxide and aldehyde products. These two products result from a competitive process between ring closure to form the epoxide product and the bimolecular reaction with O_2 ultimately leading to benzaldehyde.

76 and **77** fail to oxidize bulkier substrates such as *cis*-cyclooctene and *trans*-stylbene, illustrating the role of steric hindrance to tune this reactivity. The absence of photo-oxidation of trimethylamine (cone angle of 132°) by **76** confirms this hypothesis. By comparing the X=O bond strength (P=O, S=O, styrene oxide) of the photoproducts as a function of whether oxygen atom transfer (OAT) reactivity is observed or not, the O=Fe(IV) bond strength is evaluated to lie between 65 and 85 kcal/mol.

Excited dynamics in cofacial bisporphyrins were analyzed for **50** versus the bisporphyrin **78** and the two monoporphyrins **79**–**80** (Scheme 33) [65]. The photophysical data of these phosphorescent species are listed in Table 7.

Table 7
Photophysical data for **50**, **78**–**80** in CH_2Cl_2 at 298 K [65]

	λ_{phos} (nm)	Φ_P ($\times 10^3$)	τ_P (μs)
50	678	29(1)	102(3)
78	673	4.6(12)	18.2(2)
79	669	64(4)	321(12)
80	673	0.72(5)	1.14(1)

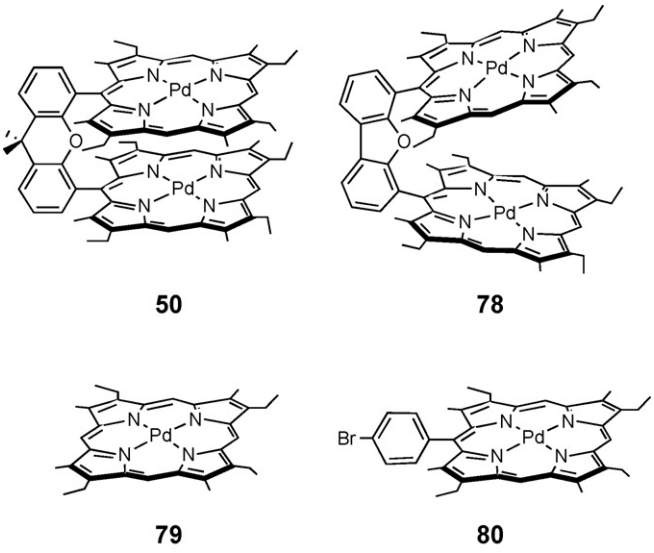

Scheme 33.

The phosphorescence band for **50** is red-shifted in comparison with the model compound **80**, which is indicative of an exciton coupling in **50**. For **78**, the smaller red-shift of the emission (and taking into account the solvent effect) indicates only a little exciton coupling in this case [65]. The exciton splittings have been evaluated at 5950 and 1410 cm^{-1} for **50** and **78**, respectively, which is consistent with the greater proximity for **50**. However, **78** should have had exhibited greater Φ_P and τ_P with regards to **50** because of inter-macrocycle interactions, similar to that reported for the corresponding free bases, **59** and **57**, respectively [54].

The presence of two absorption maxima in the ns transient spectra arising from triplet states is interpreted by the presence of two triplet states exhibiting planar and non-planar geometries [65]. This hypothesis was confirmed by DFT calculations. It is proposed that the excited state distortion about the C_{meso}–C_{aryl} bond is more accentuated for **78** than **50** leading to more deactivation in the triplet excited states.

The effect of host–guest chemistry on the excited state properties of **69** was recently investigated by X-ray crystallography, ^{1}H NMR (in CD_2Cl_2), UV–vis (in CH_2Cl_2), and ns transient absorption spectroscopy (FWHM = 3 ns at 532 nm) (Scheme 34) [66]. Addition of 2-aminopyridine (2-ampyr) to **69** induces changes in the UV–vis and ^{1}H NMR spectra where isosbestic points are obvious in the formers, and new resonances appear in the latter's. The X-ray data confirm the presence of the host–guest complex, **69**·(2-ampyr).

The comparison of the association constants (K_A) of **69** for 2-aminopyrimidine ($9.6(7) \times 10^7\ M^{-1}$), pyrimidine ($4.0(2) \times 10^4\ M^{-1}$), 2-chloropyrimidine ($6.2(1) \times 10^2\ M^{-1}$), 2-bromopyrimidine ($7.0(1) \times 10^2\ M^{-1}$), and 5-aminopyrimidine ($7.0(1) \times 10^4\ M^{-1}$) indicates that the relative basicity of the substrates alone does not explain the trend. Subtle cavity effects are believed to play a role in the host–guest stabilization.

The ns transient absorption spectra of **68**, **69**, **69**·(2-ampyr), **81** and **82** exhibit the traditional T_1–T_1 absorption known for such a chromophore (Scheme 34). The presence of an intermediate in the triplet state was confirmed by the quenching by O_2. The maxima and lifetimes of the transient absorption are 443 nm and 21.4(12) μs for **69**, and 451 nm and 227(8) μs for **69**·(2-ampyr). The large increase in transient lifetimes is consistent with an increase in scaffold rigidity. Indeed, the rotation about the C_{meso}–C_{aryl} promoting excited deactivation, is prevented when the guest molecule blocks the motion. The closer resemblance with the data for dimer **68** (τ = 169(9) μs) and the monoporphyrin **82** (τ = 161(5) μs) confirms this hypothesis.

The role of the spacer on the singlet–singlet **ET** rates and mechanisms (Förster versus Dexter) in cofacial bisporphyrins **83**–**87** was recently reported (Scheme 35) [67]. Based on the position of the 0–0 absorptions in the Q-region, the donor and acceptor are the zinc(II) porphyrin and free base chromophores, respectively.

The rate for **ET**, k_{ET}, can be calculated from $k_{ET} = (1/\tau_F) - (1/\tau_F^o)$, where τ_F and τ_F^o are the fluorescence lifetimes of the donor–acceptor dyad and donor–donor dimer [8]. The use of homo-dimers (donor–donor dimer) is necessary since the rate of excited deactivation is also function of intramolecular torsional motion as demonstrated above. For **83**–**87**, the corresponding donor–donor dimers are **89**, **68**, **88**, **90** and **69**, respectively (Scheme 36). The comparison of the fluorescence spectra of the donor–acceptor dyads with the homo-dimers shows a large decrease in donor fluorescence intensity. The blue-shifted 0–0 peak of the donor is still perceptible, despite the weak intensity as shown in Fig. 3 for the free base **58**, **86** and **90**. In this exam-

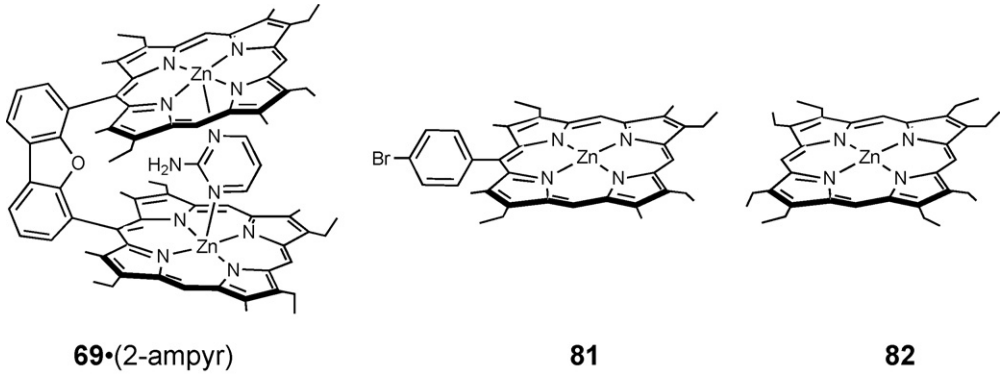

Scheme 34.

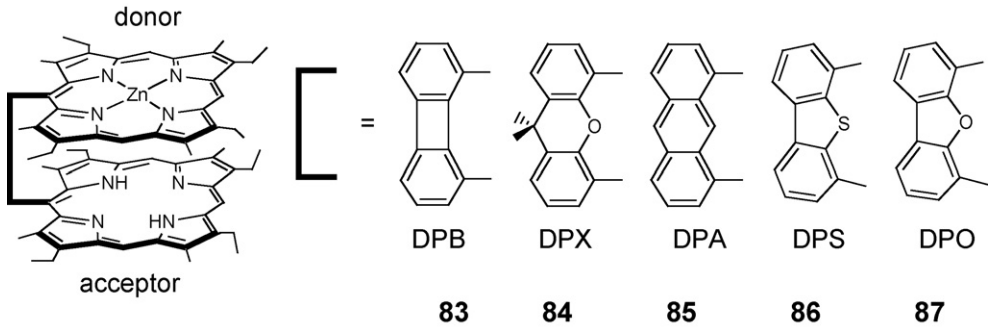

Scheme 35.

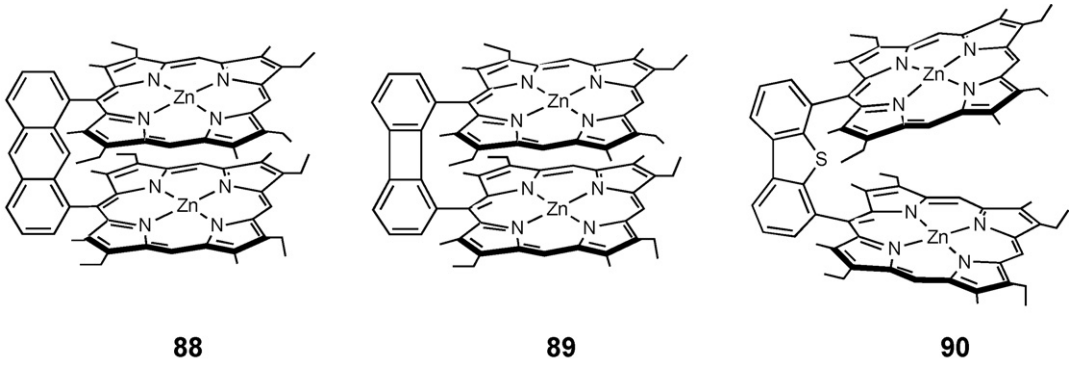

Scheme 36.

ple, the total Φ_F of **86** is approximately the sum of both Φ_F for **58** and **90**, unambiguously demonstrating the presence of **ET**.

Table 8 compares the photophysical data for **83**–**87**. There is a decrease in τ_F going from the donor–donor dimer (in parentheses) to the donor–acceptor dyad by about one order of magnitude at 298 and 77 K. These data allow to assign the **ET** process to a through space mechanism (not through bond) because dyads **84**–**87** exhibit the same number of chemical bonds between the two chromophores. There is clearly a trend between k_{ET} and the C_{meso}–C_{meso} distance. The rate increases as the distance decreases.

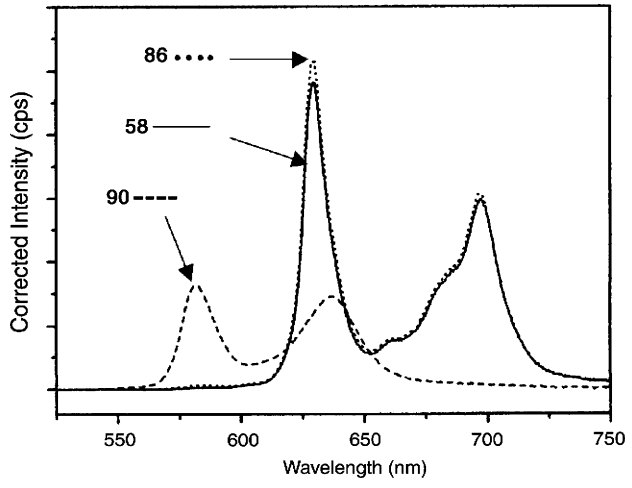

Fig. 3. Fluorescence spectra of the homo-dimers donor–donor **90** ($\Phi_F = 0.0203$), acceptor–acceptor **58** ($\Phi_F = 0.0887$), and dyad **86** ($\Phi_F = 0.1070$ total) in 2-MeTHF at 298 K (modified from Ref. [67]).

The k_{ET} data were analyzed according to the Dexter and Förster theories [68–70]. These singlet–singlet mechanisms involve a dipole–dipole interaction (Förster) and exchange process (double **et**; Dexter) that can be expressed as Eqs. (1) and (2) [68–70]:

$$k_{ET}\,(\text{Förster}) = k_D d_F^6 (1/d)^6 \quad (1)$$

$$k_{ET}\,(\text{Dexter}) = (2\pi/h) K J \exp(-2d/L) \quad (2)$$

where k_D is the emission rate constant for the donor, d_F the Förster radius, the distance at which transfer and spontaneous decay of excited donors are equally probable, d the

Table 8
τ_F and k_{ET} data for **83**–**87** in 2-MeTHF[a]

	τ_F (ns)[b]		k_{ET} (ns^{-1})		C_{meso}–C_{meso}
	298 K	77 K	298 K	77 K	(Å)[c]
83 (**89**)	0.05 (0.63)	0.06 (1.80)	20.8	15.4	3.80
84 (**68**)	0.10 (1.73)	0.09 (1.94)	9.8	10.9	4.32
85 (**88**)	0.14 (1.70)[d]	0.13 (1.94)[d]	6.4	7.2	4.94
87 (**69**)	0.18 (1.69)	0.16 (2.01)	5.0	5.9	5.53
86 (**89**)	0.19 (1.95)	0.19 (1.85)	4.7	4.6	6.33

[a] The corresponding τ_F values for the donor–donor bismacrocycles are in parentheses [67].
[b] The uncertainties are ±10%.
[c] From X-ray data listed in Ref. [67], except for **87** and **69**. In these cases, this value is from both computer modeling and X-ray data.
[d] The values in parentheses are those for (5-phenyl-2,8,13,17-tetraethyl-3,7,12,18-tetramethylporphyrin)zinc [67].

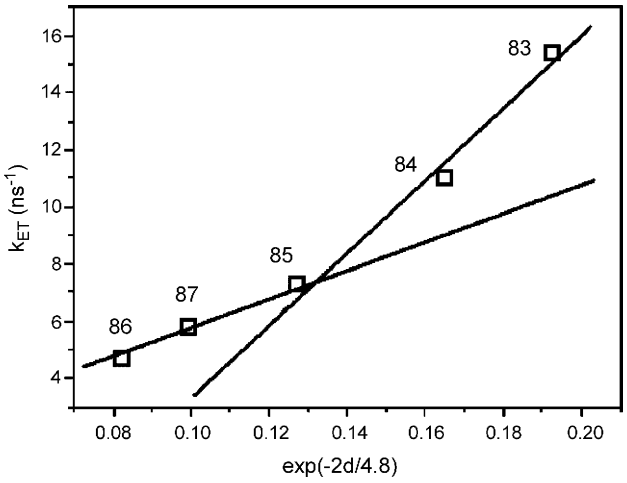

Fig. 4. k_{ET} at 77 K for **83–87** in 2-MeTHF reported against exp(−2*d*/4.8), i.e. Dexter scale (modified from Ref. [67]).

distance between the two chromophores, *J* the integral overlap, *K* an experimental constant, and *L* is the average Bohr radius (*L* = 4.8 Å for porphyrin [71]). Fig. 4 reports k_{ET} at 77 K for **83–87** in 2-MeTHF reported against exp(−2*d*/4.8) (Dexter scale for example).

This graph shows two distinct regions (**86–87**; long C_{meso}–C_{meso} distance) and (**83–84**; short C_{meso}–C_{meso} distance) with **85** being an intermediate. If the **ET** process was solely due to a Dexter mechanism, Fig. 4 would show a linear relationship. Instead, it indicates the presence of a second mechanism (i.e. Förster). A graph of k_{ET} versus $1/d^6$ exhibits the same double region behaviour. These plots clearly indicate that the k_{ET}(total) = k_{ET}(Förster) + k_{ET}(Dexter) where the change in the dominant mechanism is found at $d \sim 5$ Å. The evaluation of the critical distance where one mechanism turns over the other is unprecedented.

By changing the nature of the donor, here replacing Zn by GaOMe as in **91–93**, a similar behaviour is observed [67]. For example, k_{ET} (77 K) are 7.0, 4.8 and 6.0 ns^{-1}, respectively. In these cases, the fluorescence lifetime of the donor–donor dimer was not employed because of the presence of a double fluorescence as indicated for **37**. Instead, monomer **94** was used for all three Ga-containing materials (Scheme 37).

The rate measured at 298 K for **83** (∼21 ns^{-1}), which is the fastest in this series, is a bit less than an order of magnitude for one of the fastest rates observed so far for the linear dimer **95** (∼286 ns^{-1}) [72]. In this case, a through bond mechanism operates and the linearity of this dyad certainly helps the transfer. Can the **ET** rate be rendered faster in cofacial dyads? The answer relies on the capacity of synthesizing spacers that compress the donor and acceptor further as in **60–67** (Scheme 38).

The triplet–triplet **ET** was also investigated using series **49–51**, **56–58**, **68**, **83–84**, **86**, **89–90** and **96–108** (Scheme 39), where the population of triplet states are promoted by the heavy atoms [73]. With M = Pd and Pt, it is reasonably assumed that the quantum yield for triplet formation is nearly unity. The unique feature here is that the Förster mechanism does not operate in the triplet state due to the diradical-type excited state.

Clear evidence for triplet–triplet **ET** is obtained by examining **97** and **100**. The free base monoporphyrin chromophore, such as **105** for example, is non-phosphorescent. In **97** and **100**, a (weak) phosphorescence is observed at about 800 nm. More striking, when the excitation spectra are measured at 650 (λ_{phos} of the donor) and 800 nm (λ_{phos} of the acceptor), the former exhibits signals attributed only to the donor, while the latter shows signals

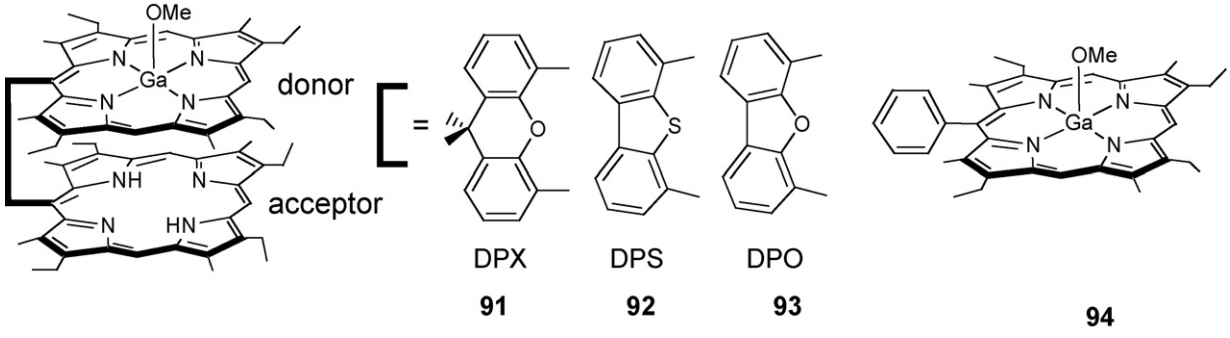

Scheme 37.

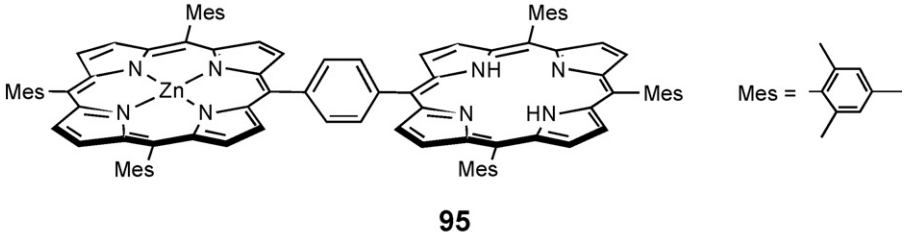

Scheme 38.

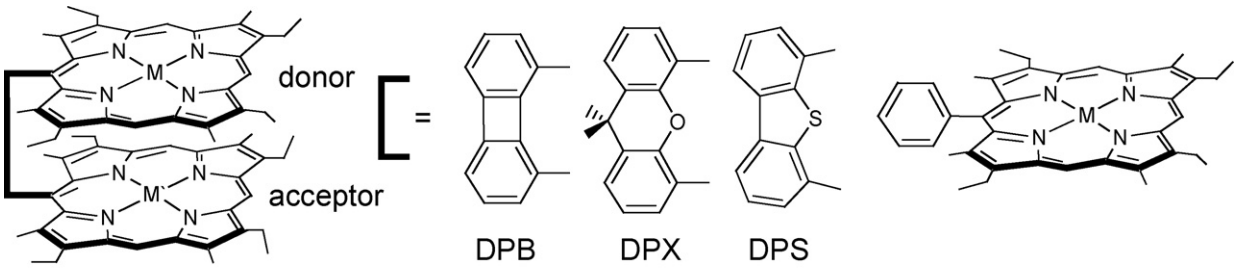

spacer	DPB	DPB	DPB	DPX	DPX	DPX	DPX	DPS	DPS
M	Pt	2H	2H	Pt	2H	2H	Zn	2H	Zn
M'	Pt	Pt	Pd	Pt	Pt	Pd	Pd	Pd	Pd
	96	**97**	**98**	**99**	**100**	**101**	**102**	**103**	**104**

Monoporphyrin:**105** (M = 2H), **106** (M = Zn), **107** (M = Pd), **108** (M = Pt)

Scheme 39.

arising from both chromophores. Only an **ET** process can adequately explain these experimental results (and not heavy atom effect). Based on the position of the phosphorescence 0–0 peaks, the Pd- and Pt-metallated chromophores act as triplet donors, whereas the free base and Zn-containing materials are the energy acceptors. The energy diagram is depicted in Fig. 5. By comparing the emission spectra of the donor–acceptor dyads with the donor–donor and acceptor–acceptor dimers (similar to Fig. 3), an evident decrease of the donor phosphorescence is observed, as well as the apparition of the acceptor phosphorescence.

The triplet–triplet k_{ET}'s are extracted in a similar manner as the singlet–singlet one ($k_{ET} = (1/\tau_P) - (1/\tau_P^o)$). Table 9 lists the key photophysical data necessary for extracting k_{ET} (data for the free bases and Zn-containing chromophores are not listed for convenience) [73]. The room temperature data are not considered in the evaluation because some data indicate an apparent absence of transfer. The fact that the excited state is distorted as indicated above may generate different conformations making the donor–donor dimers and donor–acceptor dyads geometrically different. In such cases, the comparison may be wrong. On the other hand, the conformation change in the triplet state is much more prevented in frozen matrices so that the comparison is possible.

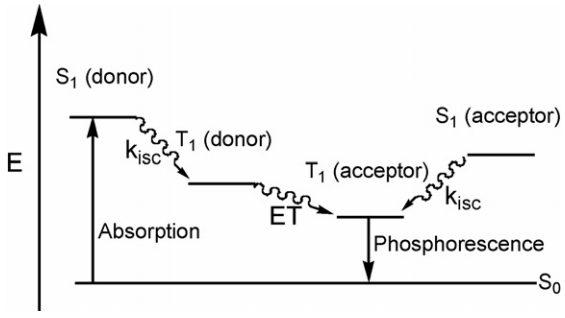

Fig. 5. Energy diagram showing the various photophysical event in triplet–triplet energy donor–acceptor dyads (k_{isc} = intersystem crossing).

The k_{ET} data presented in Table 9 can be divided into two groups: DPB- and DPX-containing dyads where transfer occurs, and DPS-containing materials where no sensitive transfer occurs or is detected. The switch where **ET** operates or not is found between DPS (C_{meso}–C_{meso} = 6.33 Å) and DPX (C_{meso}–C_{meso} = 4.32 Å). These two spacers are precisely those where the singlet–singlet **ET** occurs via a Förster and Dexter mechanism, respectively. In the triplet state the Förster process does not operate. The switch in mechanism is translated by an "all or nothing" or "on/off" situation. Such concept opens the door for the design of molecular switches based on the distance separating the donor from the acceptor.

3.3. Cofacial bisporphyrins held by the calix[4]arene spacer

The concept of designing molecular switches based on donor–acceptor separation is certainly interesting because it opens the door to applications such as measuring distances based on photophysical data and as sensors for given substrates. The calix[4]arene spacer is a flexible device but different from what is presented above. The flexibility is limited to a unique form: "open mouth" versus "closed mouth" [74,75].

Recently, compounds **109** and **110** were prepared and characterized (Scheme 40) [76]. From VT ^{1}H NMR (using CD_2Cl_2 as solvent), clear evidence for "open-closed" equilibrium is found in **110** based on the behaviour of the *meso*-protons (chemical shifts and resonance widths). At low temperature (183 K), the conformation is closed where the two macrocycles are placed face to face, whereas the conformation is open at 298 K (Fig. 6). About 10 nm red-shift of the Soret band is observed in the UV–vis spectra of **110** going from 298 to 77 K, a result consistent with a slipped cofacial organization of the two metalloporphyrins similar to a J-aggregate [8].

Based on VT ^{1}H NMR and UV–vis spectroscopy findings, compound **109** does not exhibit this "open-closed" equilibrium. It is believed to be linked to the relative flexibility of the free

Table 9
Photophysical data for the cofacial triplet–triplet **ET** dyads [73][a]

D–A dyad (D–D dimer)	Donor	Acceptor	τ_P^{donor} (μs)/298 K (τ_P D–D dimer)	τ_P^{donor} (μs)/77 K (τ_P D–D dimer)	k_{ET} (s^{-1})/77 K
97 (**96**)	Pt	2H	24 (32)	122 (136)	840
98 (**49**)	Pd	2H	368 (258)	1690 (2170)	133
100 (**99**)	Pt	2H	40.6 (46)	126 (175)	2220
101 (**50**)	Pd	2H	568 (440)	1440 (2240)	247
102 (**50**)	Pd	Zn	548 (440)	1670 (2240)	151
103 (**51**)	Pd	2H	98 (210)	1920 (1920)	0
104 (**51**)	Pd	Zn	98 (210)	1920 (1920)	0
107	Pd	–	25	1870	–
108	Pt	–	18	128	–

[a] In parentheses are the τ_P data for the homo-dimers. The solvent is 2-MeTHF.

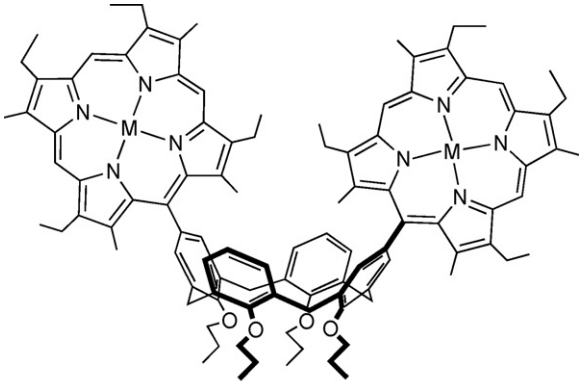

109 (M = 2H), **110**(M = Zn)

Scheme 40.

base macrocycle, preventing good "sliding" into place. The presence of methyl groups inside the cavity cause some hindrance that may cause ring deformation when the two macrocycles are close to each other. For the more rigid metalloporphyrin, such a situation is unlikely.

Another piece of evidence arises from the photophysical data (Table 10). The increase in Φ_F and τ_F in **105**, **106** and **109** going from 298 to 77 K is consistent with a typical increase in medium rigidity at low temperature. The Φ_F datum for **105** at 77 K may need to be revisited. On the other hand, for **110**, both Φ_F and τ_F unexpectedly decrease at 77 K, instead of increasing. The close proximity promotes a small (but sensitive) excited singlet state deactivation similar to what was described for **36** and **56–59** above.

With regards to the design of molecular switches, the first problem with these systems is the proximity of the β-methyl groups to the calix[4]arene macrocycle. These substituents force the porphyrin residues to be oriented at an angle with respect to the rectangular shape of the calix[4]arene macrocycle. As a consequence, the good behaviour of the molecular device is strongly bonded to steric factors. For example, **109** cannot act as a molecular switch. The second problem is the nature of the stimuli necessary to induce the conformational change. Temperature is an obvious stimuli but it is not an interesting one when one considers the temperature span necessary for this change in geometry. The wide spread in temperature observed for **110** also indicates that this system is likely not appropriate for this purpose.

In order to overcome these problems, two simple modifications can be incorporated in these "Pacman" molecules. First, the use of ethynyl groups separating the calix[4]arene aryls from the porphyrin chromophores prevents steric hindrance between the two macrocycles. Second, the use of crown ethers at the lower rim of the calix[4]arene allows to freeze the macrocycle conformation (cone shape or 1,3-alternate [74,75]) by complexing alkali cations. In this respect, a recent application in bisporphyrin chemistry was reported [77]. Indeed **111** adopts a cofacial conformation when additions of Na^+ and K^+ ions are made, where binding constants of 50 and 160 M^{-1} (^{1}H NMR), respectively, are reported, respectively. Although the fluorescence spectra remain the same before and during additions (λ_F = 648 nm; FWHM = 21 nm), Φ_F decreases with the alkali concentration until complete quenching. In the absence of alkali cations, the dimer is "open" but when complexation occurs, the face-to-face geometry is adopted to allow strong complexation (Scheme 41).

One step in this direction, the model compound **112** and the calix[4]arene-bisporphyrins **113–115** were recently designed

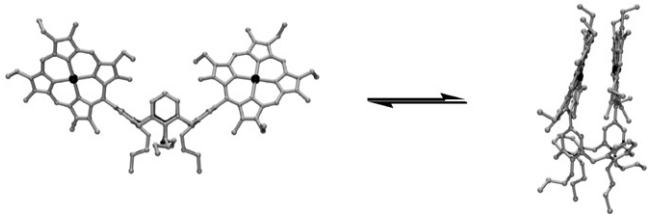

Fig. 6. "Open" to "closed" equilibrium for **110** based on computer modeling (modified from Ref. [76]).

Table 10
Fluorescence data for the calix[4]arene-containing dimers and their corresponding monoporphyrin model compounds (2-MeTHF)

Molecule	Φ_F		τ_F (ns)	
	298 K	77 K	298 K	77 K
109	0.087	0.14	17.5	23.2
105	0.089	0.086	17.3	23.3
110	0.040	0.018	1.72	1.20
106	0.0214	0.0266	1.7	1.94

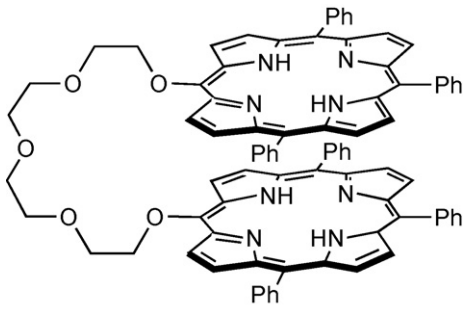

111

Scheme 41.

and investigated by UV–vis and electrochemical methods (Scheme 42) [78]. The X-ray structure of **113** exhibits an "open mouth" conformation due to crystal packing.

However, binding studies of **113–115** with diazabicyclo[2.2.2]octane (dabco) and 1,4-pyrazine demonstrate the ability to "close the mouth" allowing host–guest complexation via Zn–N coordination bonding [78], similar to **69**·(2-ampyr) [66]. The binding constants measured for the molecular tweezers **113** and **114** with these two guest substrates, in a 1:1 ratio, varies from 0.9×10^6 to 7×10^8 M^{-1}. This trend shows the relatively strong association where dabco acts as a stronger binder than 1,4-pyrazine. These systems closely resemble to those reported for the more rigid DPA-containing tweezers **116** and **117** (Scheme 43) [79]. The complex **117**·(1,4-pyrazine) exhibits an association constant of $10^{5.6}$ M^{-1} (UV–vis titration), a lower constant (10^7 M^{-1}) compared to the dabco one.

All in all, the **113–115** tweezer systems exhibit great potential for alkali cation sensing, but studies and analyses of the photophysical properties have yet to be performed.

3.4. Cofacial bisporphyrins held by a metal–metal bond

The M_2 bond is a special spacer since this covalent linking mode does not involve carbon-based architecture, and yet $d\pi$–$d\pi$ and $d\sigma$–$d\sigma$ interactions can potentially provide the necessary electronic communication between the π-systems to

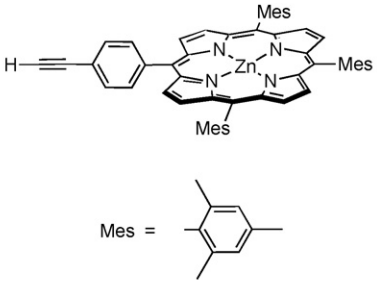

112

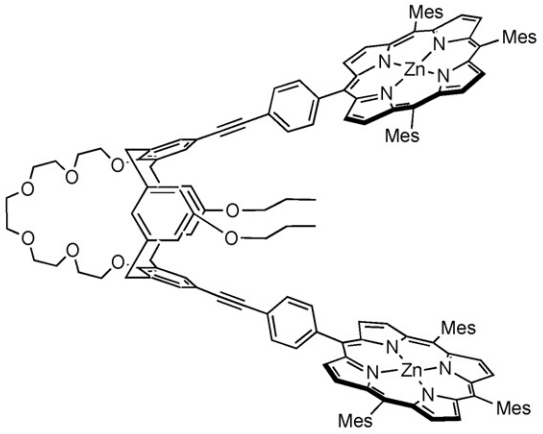

113

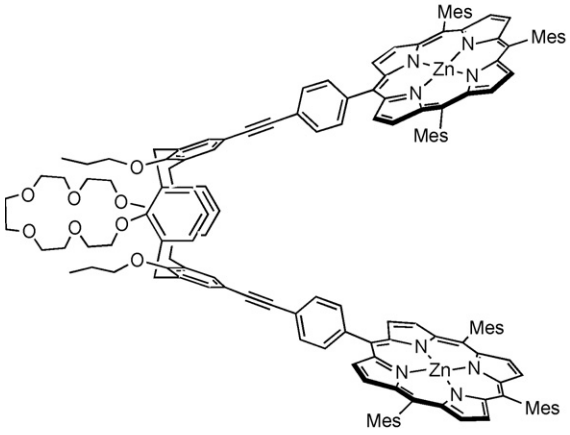

114

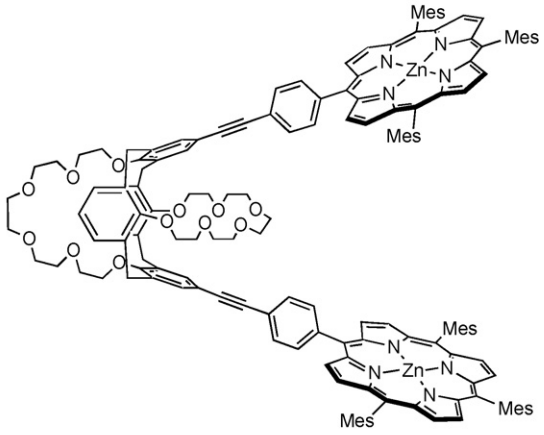

115

Scheme 42.

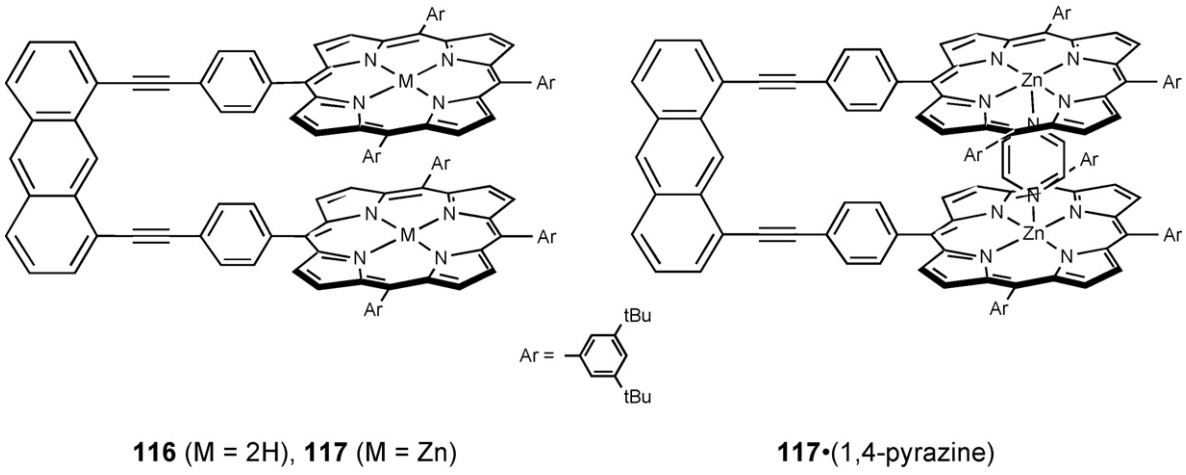

Scheme 43.

promote strong coupling, in opposition to saturated aliphatic spacers. In addition, because the M_2 bond length is significantly shorter than the sum of the van der Waals radii of the carbon atom, strong cofacial π–π contacts are clearly possible. If so, then broadening of the absorption and emission bands should be observed as described for the series **36** and **56–59**. This is particularly well exemplified with dimers **118–119** (Scheme 44), where a Ru≡Ru triple bond is established by X-ray crystallography (**118**: $d(Ru_2) = 2.166(1)$ Å) and resonance Raman spectroscopy (**119**: $\nu(Ru_2) = 317\ cm^{-1}$) [80,81]. Both the Soret and Q-bands are unusually broad [81], even at 77 K (Fig. 7) where the position of the 0–0 absorption in the Q-region cannot be localized whatsoever. Although the spectra in Fig. 7 have yet to be analyzed, the apparition of a second strong absorption band at 338 nm, beside the Soret band at 402 nm, suggests the presence of a strong exciton coupling ($4710\ cm^{-1}$) [44], which would be among the largest known in polyporphyrins and arrays [8,82].

Bisporphyrins held by a M_2 bond, as either single or multiple bonds, were known for quite a long time [83]. Surprisingly, the photophysics and photochemistry of such species have not been explored in detail. The few rare examples are described below.

The dative Rh(I) → In(III) dyads **120–123** exhibit easy photochemical decomposition at room temperature (Scheme 45) [84–87]. For example (OEP)Rh–In(OEP) **123** photoreacts with CH_3I to produce (OEP)Rh–CH_3 and I–In(OEP). This reaction is much slower when performed in the absence of light [87]. Based on the UV–vis spectral monitoring of the time necessary to observe complete decomposition of **120–123**, the relative bond strength was evaluated to be **123 < 121 < 122 < 120** [84,86]. It is believed that the excited state of the (TPP)Rh–In(TTP) molecule is the highest, and so the Rh–In bond is stronger.

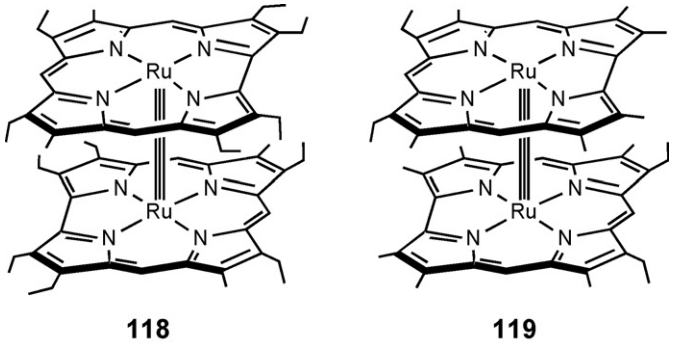

Scheme 44.

121, which appears not to be luminescent at 298 K, was investigated by means of ps–μs transient spectroscopy at 355 nm excitation [85]. The homolytic photoinduced bond cleavage appears within 20 ps of the laser pulse. Using CH_2Cl_2, the scavenging of the radical intermediates at 600 nm (forming the corresponding chlorometallo-monoporphyrins) occurs at an evolving rate with a constant of $4.1 \times 10^{10}\ M^{-1}\ s^{-1}$, a value that is at the sub-diffusion limit. Because the rate constant for recovery is concentration-dependent, recombination and scrambling reactions of the photo-fragments occur (i.e. formation of the parent homo-dimers). The absence of luminescence was, with reserve, suggested to be related to the photoinduced M–M′ bond scission in the excited state.

To our knowledge, the only work on the photophysics of M–M′-bonded species appeared this year [88]. Indeed, dyad

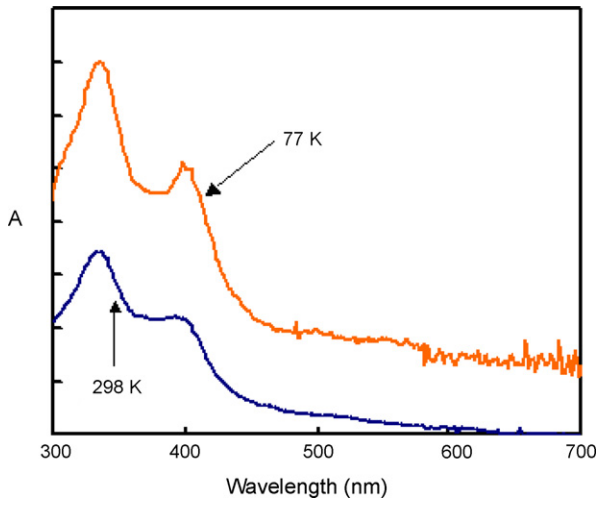

Fig. 7. UV–vis spectra of **119** in 2-MeTHF at 77 K and 298 K (an arbitrary value of 0.2 was added to the 77 K spectrum for better comparison) [80].

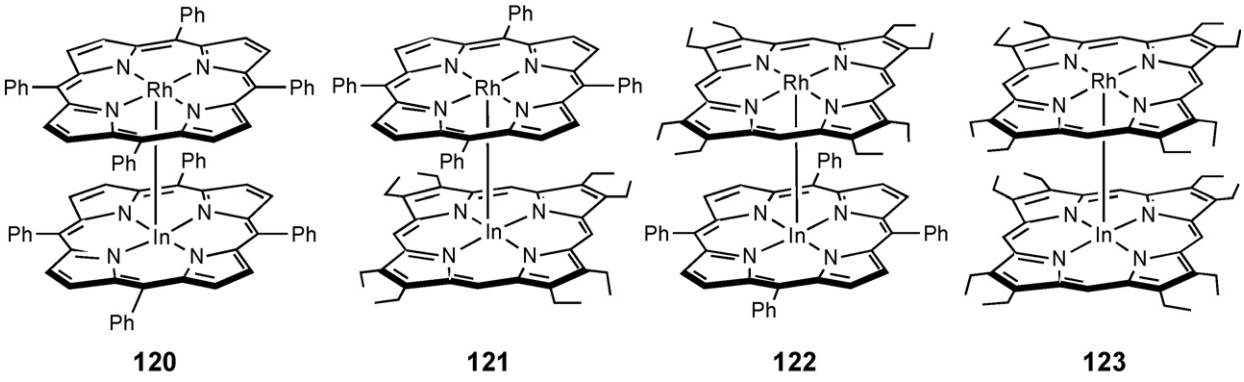

Scheme 45.

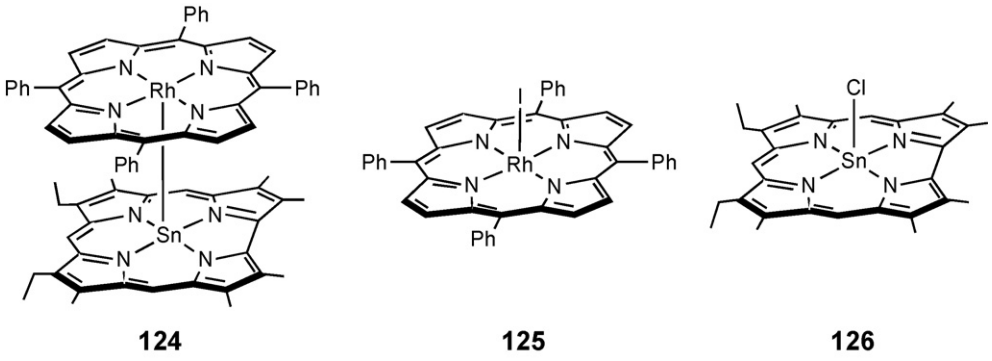

Scheme 46.

124 (rhodium *meso*-tetraphenylporphyrin-tin(2,3,7,13,17,18-hexamethyl-8,12-diethylcorrole)) exhibits a Rh–Sn bond, presumably of the same type as the Rh(I) → In(III) (i.e. Rh(I) → Sn(IV)), with a bond length of 2.5069(7) Å (Scheme 46) [89]. The average separation between the macrocycle planes is 3.4 Å; a distance below the sum of the van der Waals radii (3.54 Å). Strong inter-macrocycle interactions are anticipated.

The compound is not luminescent at 298 K, presumably for the same reason as that suspected for **120**–**123**. In frozen 77 K matrices, **124** is weakly phosphorescent, again presumably because the photoinduced M–M′ bond scission is much less efficient in more rigid media. The emission bands, as well as τ_e and Φ_e at 77 K (in 2-MeTHF as solvent), were compared to those of **125** and **126** (Scheme 46), which are the two chemical precursors of **124**. Using the absorption, fluorescence and phosphorescence spectra, the energy diagram has been established (Fig. 8).

Based on this diagram, one notes that the TPP- and corrole-containing chromophores are, respectively, the energy donor and acceptor, in both the singlet and triplet excited states. Because of the presence of heavy atoms, the triplet states are strongly populated during excitation, presumably with quantum efficiency near to 1.0. The total absence of fluorescence in **124** (while weak fluorescence is observed in the tin derivative **126**) indicates efficient excited state deactivation due to intramolecular **ET**. The large decreases in τ_P and Φ_P of the Rh(TPP) chromophore going from **125** to **124**, indicate a significant intramolecular triplet–triplet **ET** in **124** with an estimated k_{ET} ranging between 10^6 and 10^8 s^{-1} (Table 11).

The comparison of triplet–triplet k_{ET} for **124**, with those for **97**, **98**, **100** and **101**, for which a through space mechanism was demonstrated, is presented in Scheme 47. k_{ET} for **124** is much larger than the others by three to five orders of magnitude. This difference cannot be explained by a simple change in inter-chromophore distances since the change in k_{ET} is only two- to three-folds between the DPB- and DPX-spacers (3.80 Å versus 4.32 Å).

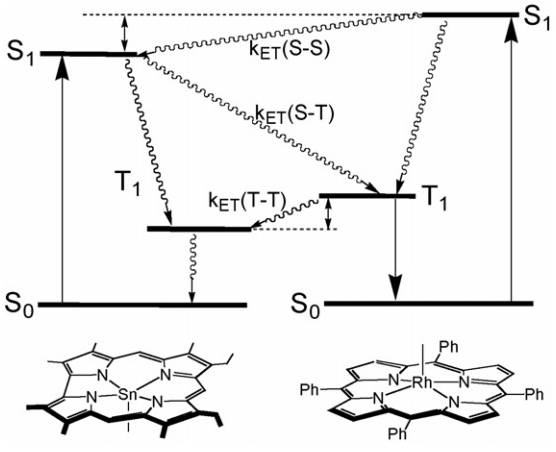

Fig. 8. Qualitative energy diagram for **124** showing the various observed radiative processes (straight line arrows) and non-radiative paths (wave-lines) [88].

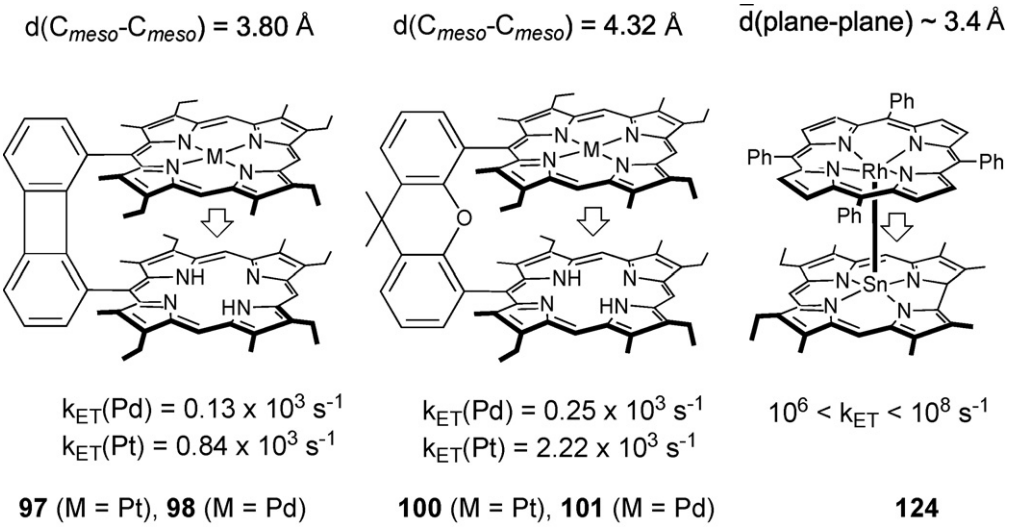

Scheme 47.

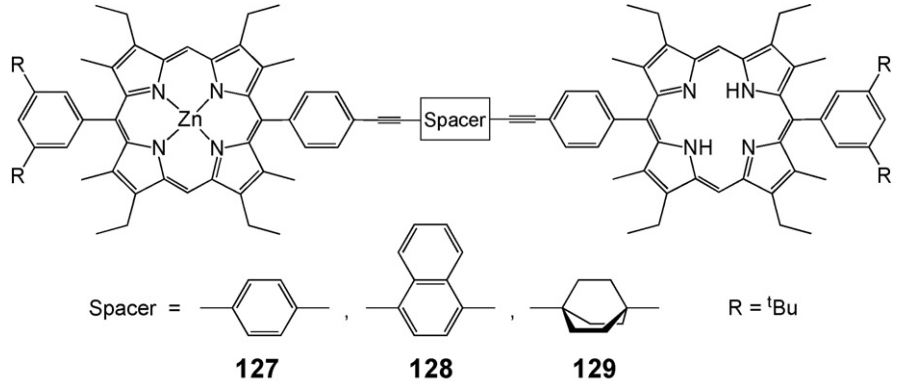

Scheme 48.

Instead, a through-bond mechanism is invoked to explain the fast rate; a rate that is one of the fastest triplet–triplet **ET** ever reported [8]. For example, **127**–**129** in 2-MeTHF at 80 K exhibit triplet–triplet k_{ET} (Zn-porphyrin = D; free base = A) of 4×10^4, 2×10^5, and $<0.1\ s^{-1}$, respectively (Scheme 48) [90,91]. This comparison helps assigning a through bond versus through space **ET** for systems exhibiting very similar D–A distances, but also shows the large change in k_{ET} (>5 orders of magnitude), similar to that seen in **124**.

Also, the closely placed cofacial systems (**97**, **98**, **100**, **101**, and **124**) show triplet–triplet through-space and through-bond k_{ET} rates that are two to three orders of magnitude faster than that of **127**–**129**, illustrating the importance of the proximity of the D–A fragments. Such a comparison may be helpful in predicting k_{ET} for unknown systems.

All in all, **124** is the first and only example of an **ET** dyad where the process takes place through a M–M bond.

Table 11
τ_e and Φ_e data for **124**–**126** (2-MeTHF/77 K) [88]

Compound	Φ_{Fluo} ($\times 10^{-3}$)	Φ_{Phos} ($\times 10^{-3}$)	τ_{Fluo} (ps)	τ_{Phos} (ns)
124[a]	–[b]	0.42 ± 0.04	–[b]	120 ± 5
125	–[b]	42 ± 4	–[b]	300 ± 5
126	9.4 ± 0.9	1.1 ± 0.1	140 ± 50	–[c]

[a] The luminescence arises from the Rh(TPP) only.
[b] Not observed.
[c] Too weak to be measured.

4. Conclusion

Cofacial bisporphyrin systems have been exhaustively investigated. Originally, the aim was to model the primary photophysical biological events occurring in LH1, LH2 and LH3 and the reaction center, where energy and electron transfer processes take place. Over the years, these "simple" bimolecular devices were modified for the design of molecular tweezers via supramolecular interactions and molecular recognition. These molecular devices were also used as photo-catalysts, but only a limited number of such systems were investigated. In addition, a through M_2-bond **ET** process was recently discovered and much more research is expected in this area, mainly from a theoretical stand point. This could be used to determine the difference between a transfer occurring through a carbon- and metal-based architecture. Applications in sensors, particularly for metallic cations such as lanthanides and actinides through the measurement of k_{ET} in crown ether-containing devices, are

also anticipated. Finally, the eventual and particularly useful estimation of the D–A separations as a function of various experimental conditions (such as various solvents and temperatures) using this type of measurements and the comparison with appropriate standards can be foreseen as the next step to be taken in this area.

Acknowledgements

The Natural Sciences and Engineering Research Council of Canada (NSERC; PDH) and the Centre National de Recherche Scientifique (CNRS; RG, CS and CG, UMR 5633) are acknowledged for funding over the years in this area of research. The authors thank the undergraduate, graduate students, and postdoctoral fellows that did the work.

References

[1] S. Karrasch, P.A. Bullough, R. Ghosh, EMBO J. 14 (1995) 631.
[2] J. Koepke, X. Hu, C. Muenke, K. Schulten, H. Michel, Structure 4 (1996) 581.
[3] G. McDermott, S.M. Prince, A.A. Freer, A.M. Hawthornthwaite-Lawless, M.Z. Papiz, R.J. Cogdell, N.W. Isaacs, Nature 374 (1995) 517.
[4] K. McLuskey, S.M. Prince, R.J. Cogdell, N.W. Isaacs, Biochemistry 40 (2001) 8783.
[5] H. Savage, M. Cyrklaff, G. Montoya, W. Kühlbrandt, I. Sinning, Structure 4 (1996) 243.
[6] T. Walz, S.J. Jamieson, C.M. Bowers, P.A. Bullough, C.N. Hunter, J. Mol. Biol. 282 (1998) 833.
[7] A.W. Roszak, T.D. Howard, J. Southall, A.T. Gardiner, C.J. Law, N.W. Isaacs, R.J. Cogdell, Science 302 (2003) 1969.
[8] See for example: P.D. Harvey, in: K.M. Kadish, K.M. Smith, R. Guilard (Eds.), The Porphyrin Handbook, vol. 18, Academic Press, San Diego, 2003, pp. 63–250, and the references therein.
[9] X. Peng, N. Aratani, A. Takagi, T. Matsumoto, T. Kawai, I.-W. Hwang, T.K. Ahn, D. Kim, A. Osuka, J. Am. Chem. Soc. 126 (2004) 4468.
[10] R. Takahashi, Y. Kobuke, J. Am. Chem. Soc. 125 (2003) 2372.
[11] D. Kim, A. Osuka, Acc. Chem. Res. 37 (2004) 735.
[12] E.I. Zen'kevich, A.S. Starukhin, A.M. Shul'ga, J. Appl. Spectrosc. 66 (1999) 544.
[13] J. Wojaczynski, L. Latos-Grazynski, Coord. Chem. Rev. 204 (2000) 113.
[14] J. Otsuki, Trends Phys. Chem. 8 (2001) 61.
[15] N. Armaroli, J.-C. Chambron, J.-P. Collin, C.O. Dietrich-Buchecker, L. Flamigni, J.-M. Kern, J.-P. Sauvage, in: V. Balzani (Ed.), Electron Transfer in Chemistry; Biological and Artificial Supramolecular Systems, vol. 3, Wiley–VCH Verlag GmbH, Weinheim, 2001, p. 582 (Chapter 8).
[16] E. Alessio, E. Iengo, L.G. Marzilli, Supramol. Chem. 14 (2002) 103.
[17] J.-C. Chambron, J.-P. Collin, I. Dixon, V. Heitz, X.J. Salom-Roig, J.-P. Sauvage, J. Porphyrins Phthalocyanines 8 (2004) 82.
[18] Y. Kobuke, J. Porphyrins, J. Porphyrins Phthalocyanines 8 (2004) 156.
[19] A. Satake, Y. Kobuke, Tetrahedron 61 (2005) 13.
[20] N. Aratani, A. Osuka, Bull. Chem. Soc. Jpn. 74 (2001) 1361.
[21] N.V. Konovalova, R.P. Evstigneeva, V.N. Luzgina, Russ. Chem. Rev. 70 (2001) 939.
[22] N. Aratani, A. Osuka, H.S. Cho, D. Kim, J. Photochem. Photobiol. C 3 (2002) 25.
[23] D. Holten, D.F. Bocian, J.S. Lindsey, Acc. Chem. Res. 35 (2002) 57.
[24] A. Prodi, M.T. Indelli, C.J. Kleverlaan, E. Alessio, F. Scandola, Coord. Chem. Rev. 229 (2002) 51.
[25] C.M. Drain, J.T. Hupp, K.S. Suslick, M.R. Wasielewski, X. Chen, J. Porphyrins Phthalocyanines 6 (2002) 243.
[26] T.S. Balaban, in: H.S. Nalwa (Ed.), Encyclopedia of Nanoscience and Nanotechnology, vol. 4, American Scientific Publishers, 2004, p. 505.
[27] D. Gust, T.A. Moore, in: K.M. Kadish, K.M. Smith, R. Guilard (Eds.), The Porphyrin Handbook, vol. 8, Academic Press, Burlington, MA, 2000, p. 153.
[28] I. Okura, Photosensitization of Porphyrins and Phthalocyanines, Kodansha, Gordon and Breach Science Publishers, Tokyo, Amsteldijk, 2000.
[29] C.K. Chang, J. Heterocycl. Chem. 14 (1977) 1285.
[30] T.L. Netzel, P. Kroger, C.K. Chang, I. Fujita, J. Fajer, Chem. Phys. Lett. 67 (1979) 223.
[31] T.L. Netzel, M.A. Bergkamp, C.K. Chang, J. Am. Chem. Soc. 104 (1982) 1952.
[32] M.R. Wasielewski, M.P. Niemczyk, W.A. Svec, Tetrahedron Lett. 23 (1982) 3215.
[33] Y. Sakata, S. Nishitani, N. Nishimizu, S. Misumi, A.R. McIntosh, J.R. Bolton, Y. Kanda, A. Karen, T. Okada, N. Mataga, Tetrahedron Lett. 26 (1985) 5207.
[34] J.A. Cowan, J.K.M. Sanders, G.S. Beddard, R.J. Harrison, J. Chem. Soc., Chem. Commun. (1987) 55.
[35] P. Leighton, J.A. Cowan, R.J. Abraham, J.K.M. Sanders, J. Org. Chem. 53 (1988) 733.
[36] C.A. Hunter, P. Leighton, J.K.M. Sanders, J. Chem. Soc., Perkin Trans. 1 (1989) 547.
[37] R. Karaman, T.C. Bruice, J. Org. Chem. 56 (1991) 3470.
[38] T.H. Tran-Thi, J.F. Lipskier, P. Maillard, M. Momenteau, J.-M. Lopez-Castillo, J.-P. Jay-Gerin, J. Phys. Chem. 96 (1992) 1073.
[39] J.M. Zaleski, C.K. Chang, G.E. Leroi, R.I. Cukier, D.G. Nocera, J. Am. Chem. Soc. 114 (1992) 3564.
[40] I. Fujita, J. Fajer, C.K. Chang, C.B. Wang, M.A. Bergkamp, T.L. Netzel, J. Phys. Chem. 86 (1982) 3754.
[41] J.M. Zaleski, C.K. Chang, D.G. Nocera, J. Phys. Chem. 97 (1993) 13206.
[42] J.L. Sessler, E.A. Brucker, V. Kral, A. Harriman, Supramol. Chem. 4 (1994) 35.
[43] V.V. Borovkov, J.M. Lintuluoto, M. Sugiura, Y. Inoue, R. Kuroda, J. Am. Chem. Soc. 124 (2002) 11282.
[44] Unpublished results.
[45] A. Osuka, K. Maruyama, N. Mataga, T. Asahi, I. Yamazaki, N. Tamai, Y. Nishimura, Chem. Phys. Lett. 181 (1991) 413.
[46] A. Osuka, T. Nagata, K. Maruyama, Chem. Lett. (1991) 481.
[47] H.A. Staab, T. Carell, Angew. Chem. Int. Ed. 33 (1994) 1466.
[48] P.D. Harvey, N. Proulx, G. Martin, M. Drouin, D.J. Nurco, K.M. Smith, F. Bolze, C.P. Gros, R. Guilard, Inorg. Chem. 40 (2001) 4134.
[49] O. Ohno, Y. Kaizu, H. Kobayashi, J. Chem. Phys. 82 (1985) 1779.
[50] F. Bolze, M. Drouin, P.D. Harvey, C.P. Gros, E. Espinosa, R. Guilard, J. Porphyrins Phthalocyanines 7 (2003) 474.
[51] F. Bolze, C.P. Gros, P.D. Harvey, R. Guilard, J. Porphyrins Phthalocyanines 5 (2001) 569.
[52] S. Faure, C. Stern, R. Guilard, P.D. Harvey, Inorg. Chem. 44 (2005) 9232.
[53] C.K. Chang, I. Abdalmuhdi, Angew. Chem. Int. Ed. 23 (1984) 164.
[54] F. Bolze, C.P. Gros, M. Drouin, E. Espinosa, P.D. Harvey, R. Guilard, J. Organomet. Chem. 643/644 (2002) 89.
[55] J.T. Fletcher, M.J. Therien, J. Am. Chem. Soc. 124 (2002) 4298.
[56] Y. Shimazaki, H. Takesue, T. Chishiro, F. Tani, Y. Naruta, Chem. Lett. (2001) 538.
[57] A. Osuka, S. Nakajima, T. Nagata, K. Maruyama, K. Toriumi, Angew. Chem. Int. Ed. 30 (1991) 582.
[58] J.T. Fletcher, M.J. Therien, Inorg. Chem. 41 (2002) 331.
[59] J.T. Fletcher, M.J. Therien, J. Am. Chem. Soc. 122 (2000) 12393.
[60] M. Gouterman, in: D. Dolphin (Ed.), The Porphyrins, vol. III, Academic Press, New York, 1978, p. 1.
[61] C.J. Chang, E.A. Baker, B.J. Pistorio, Y. Deng, Z.-H. Loh, S.E. Miller, S.D. Carpenter, D.G. Nocera, Inorg. Chem. 41 (2002) 3102.
[62] J.M. Hodgkiss, C.J. Chang, B.J. Pistorio, D.G. Nocera, Inorg. Chem. 42 (2003) 8270.
[63] B.J. Pistorio, C.J. Chang, D.G. Nocera, J. Am. Chem. Soc. 124 (2002) 7884.
[64] J. Rosenthal, B.J. Pistorio, L.L. Chng, D.G. Nocera, J. Org. Chem. 70 (2005) 1885.
[65] Z.-H. Loh, S.E. Miller, C.J. Chang, S.D. Carpenter, D.G. Nocera, J. Phys. Chem. A 106 (2002) 11700.

[66] C.J. Chang, Z.-H. Loh, Y. Deng, D.G. Nocera, Inorg. Chem. 42 (2003) 8262.
[67] S. Faure, C. Stern, R. Guilard, P.D. Harvey, J. Am. Chem. Soc. 126 (2004) 1253.
[68] D.L. Dexter, J. Chem. Phys. 21 (1953) 836.
[69] T. Förster, Naturwissenschaften 33 (1946) 166.
[70] T. Förster, Ann. Phys. (San Diego) 2 (1948) 55.
[71] J.P. Fillers, K.G. Ravichandran, I. Abdalmuhdi, A. Tulinsky, C.K. Chang, J. Am. Chem. Soc. 108 (1986) 417.
[72] S.I. Yang, R.K. Lammi, J. Seth, J.A. Riggs, T. Arai, D. Kim, D.F. Bocian, D. Holten, J.S. Lindsey, J. Phys. Chem. B 102 (1998) 9426.
[73] S. Faure, C. Stern, E. Espinosa, J. Douville, R. Guilard, P.D. Harvey, Chem. Eur. J. 11 (2005) 3469.
[74] P.D. Harvey, Coord. Chem. Rev. 233/234 (2002) 289.
[75] P.D. Harvey, J. Inorg. Organomet. Polym. 14 (2004) 211.
[76] J.-P. Tremblay-Morin, S. Faure, D. Samar, C. Stern, R. Guilard, P.D. Harvey, Inorg. Chem. 44 (2005) 2836.
[77] D. Monti, M. Venanzi, G. Mancini, F. Marotti, L.L. Monica, T. Boschi, Eur. J. Org. Chem. (1999) 1901.
[78] D. Jokic, C. Boudon, G. Pognon, M. Bonin, K.J. Schenk, M. Gross, J. Weiss, Chem. Eur. J. 11 (2005) 4199.
[79] J. Brettar, J.-P. Gisselbrecht, M. Gross, N. Solladié, Chem. Commun. (2001) 733.
[80] P.D. Harvey, S. Sicard, F. Burdet, J.-M. Barbe, R. Guilard, Can. J. Anal. Sci. Spectrosc. 48 (2003) 121.
[81] F. Jérôme, B. Billier, J.M. Barbe, E. Espinosa, S. Dahaoui, C. Lecomte, R. Guilard, Angew. Chem. Int. Ed. 39 (2000) 4051.
[82] N. Aratani, A. Osuka, Y.H. Kim, D.H. Jeong, D. Kim, Angew. Chem. Int. Ed. 39 (2000) 1458.
[83] J.P. Collman, H.J. Arnold, Acc. Chem. Res. 26 (1993) 586.
[84] D. Lux, D. Daphnomili, A.G. Coutsolelos, Polyhedron 13 (1994) 2367.
[85] A.G. Coutsolelos, D. Daphnomili, W.R. Scheidt, G. Ferraudi, Inorg. Chem. 37 (1998) 2077.
[86] A.G. Coutsolelos, D. Lux, E. Mikros, Polyhedron 15 (1996) 705.
[87] N.L. Jones, P.J. Carroll, B.B. Wayland, Organometallics 5 (1986) 33.
[88] J. Poulin, C. Stern, R. Guilard, P.D. Harvey, Photochem. Photobiol. 82 (2006) 171.
[89] J.-M. Barbe, G. Morata, E. Espinosa, R. Guilard, J. Porphyrins Phthalocyanines 7 (2003) 120.
[90] K. Kilså, J. Kajanus, J. Mårtensson, B. Albinsson, J. Phys. Chem. B 103 (1999) 7329.
[91] J. Andreasson, J. Kajanus, J. Mårtensson, B. Albinsson, J. Am. Chem. Soc. 122 (2000) 9844.